https://doi.org/10.5194/egusphere-2026-4647
Preprint. Discussion started: 2 September 2026

Climatology and trends in stratospheric mean age of air from correlations of multiple trace gases measured by ACE-FTS

Florian Voet[1,2], Felix Ploeger[1,2], Johannes C. Laube[1], Laura N. Saunders[3], Patrick E. Sheese[3], Attahir Mainika[1], Peter Preusse[1], Jens-Uwe Grooß[1], Kaley A. Walker[3], Susann Tegtmeier[4], and Michaela I. Hegglin[1,2,5]

[1]Institute of Climate and Energy Systems: Stratosphere (ICE-4), Forschungszentrum Jülich, Jülich, Germany
[2]Institute for Atmospheric and Environmental Research, University of Wuppertal, Wuppertal, Germany
[3]Department of Physics, University of Toronto, Toronto, Canada
[4]Institute of Space and Atmospheric Studies, University of Saskatchewan, Saskatoon, Canada
[5]Department of Meteorology, University of Reading, Reading, UK

Correspondence: Florian Voet (f.voet@fz-juelich.de)

Abstract. We develop and apply a novel method for estimating stratospheric mean age of air (AoA) from trace gases observed by the Atmospheric Chemistry Experiment – Fourier Transform Spectrometer (ACE-FTS). The method combines SF_6 with five additional long-lived tracers, N_2O, CH_4, CFC-11, CFC-12, and HCFC-22, and is evaluated for ACE-FTS dataset versions 3.6 and 5.2. A proof of concept using the Chemical Lagrangian Model of the Stratosphere (CLaMS) shows that the multi-tracer approach reduces the uncertainty of zonal-mean AoA by about 50% relative to conventional methods based only on SF_6 and yields AoA estimates at individual profiles with an average uncertainty of about 0.3 years. Applied to ACE-FTS data, the multi-tracer method produces smoother AoA fields and strongly suppresses noise in sparsely sampled regions compared with the conventional convolution method. Comparison with in situ AoA estimates from SF_6 and CO_2 generally favors the multi-tracer product, although some discrepancies remain. The method provides a precise and spatially resolved satellite-based AoA product and a promising basis for future studies of long-term changes in stratospheric circulation. Comparison of ERA5 AoA with the new satellite product indicates a slow bias in the reanalysis. The long-term AoA trend pattern over 2004–2021 shows increasing age in the Northern Hemisphere stratosphere between about 18–28 km and decreasing age in the tropics and Southern Hemisphere subtropics, largely consistent with ERA5. In particular, AoA increases in the Northern relative to the Southern Hemisphere.

1 Introduction

The Brewer–Dobson circulation (BDC) is the large-scale meridional overturning circulation of the stratosphere, characterized by tropical upwelling, poleward transport, and descent in the extratropics. It governs the distribution of long-lived, radiatively active gases, as well as ozone, throughout the stratosphere, thereby influencing the global radiation budget and playing a key role in Earth's climate system.

With vertical circulation velocities on the order of millimeters per second, the BDC is roughly three orders of magnitude slower than typical horizontal winds and cannot be measured directly. Instead, its strength is inferred from observations of

https://doi.org/10.5194/egusphere-2026-4647
Preprint. Discussion started: 2 September 2026

long-lived trace gases transported by the circulation. First conceptualized by Kida (1983a, b) and later formally defined by Hall and Plumb (1994), the stratospheric mean age of air (AoA) has become the standard diagnostic for quantifying the strength of the BDC (for a recent review see Garny et al., 2024b).

AoA is defined as the average time elapsed since the air parcel at a given location and time in the stratosphere last contacted a specified boundary region, typically the tropical tropopause or tropical surface region. For an ideal clock tracer — i.e., a trace gas with a linearly increasing mixing ratio at the boundary that is free of sources and sinks elsewhere — AoA can be determined exactly by matching the observed stratospheric mixing ratio to its historical record at the boundary and calculating the corresponding time lag (Hall and Plumb, 1994).

Due to varying tropospheric emission rates and upper atmospheric sink reactions, however, only approximate clock tracers exist in the real atmosphere, for which a simple lag-time estimate does not accurately represent AoA without further corrections. Prominent examples of such approximate clock tracers include sulfur hexafluoride (SF_6) and carbon dioxide (CO_2), for which established methods are used to infer AoA (Volk et al., 1997; Ray et al., 2014; Garny et al., 2024b). In addition, Leedham Elvidge et al. (2018) demonstrated the applicability of certain perfluorocarbons and hydrofluorocarbons for AoA estimation using similar approaches.

While these so-called age tracers can be measured with relatively low uncertainty using in situ instruments, their retrieval from remote sensing observations is subject to substantially larger uncertainties. For satellite-based measurements, SF_6 is currently the only trace gas that can be used to estimate AoA directly with well-established standard methods. However, the uncertainty of satellite-based SF_6 retrievals is still too large to estimate AoA at individual retrieval grid points; instead, averages over a sufficiently large number of measurements are required to reduce noise. As a result, only zonal-mean AoA estimates based on satellite SF_6 observations have been published so far (Stiller et al., 2012; Saunders et al., 2025; Haenel et al., 2015).

The uncertainties in age of air estimates from satellite trace gas observations are particularly important when it comes to deducing long-term trends, to investigate potential changes in the stratospheric circulation. In this respect, even mean age estimates from the same satellite data but derived with different methods have been recently shown to result in different trends (Dubé et al., 2025; Saunders et al., 2025). Also for in situ observations it is challenging to infer age trends, as these observations have sparse sampling and for long timeseries data from different instruments needs to be merged (Ray et al., 2026). Notwithstanding these difficulties, trends in mean age of air and in the stratospheric circulation are an important factor in the climate system as they may be related to trends in radiatively active trace gas species. On longer timescales, observational age estimates do not agree with the robust climate model prediction of decreasing age and an accelerating stratospheric circulation with global warming. On decadal timescale, additional factors of natural climate variability play a role and it appears that these have caused a hemispheric asymmetry in decadal changes of age of air and circulation (Strahan et al., 2020; Ploeger and Garny, 2022). An independent estimate of these potential changes from satellite observations is highly valuable for constraining changes in stratospheric circulation.

Given these challenges, other long-lived tracers that are retrieved with lower uncertainty and correlate tightly with AoA have also been used to estimate AoA, although additional information is still required. Linz et al. (2017) and, more recently, Castillo et al. (2026) used satellite-based nitrous oxide (N_2O) to derive AoA from empirical relationships between N_2O and

https://doi.org/10.5194/egusphere-2026-4647
Preprint. Discussion started: 2 September 2026

AoA inferred from CO_2 and SF_6 (e.g. Andrews et al., 2001). Dubé et al. (2025) used satellite-based measurements from the Atmospheric Chemistry Experiment–Fourier Transform Spectrometer (ACE-FTS) of N_2O, methane (CH_4), and dichlorodifluoromethane (CFC-12), in combination with results from the Chemical Lagrangian Model of the Stratosphere (CLaMS), to derive long-term trends of AoA.

In a previous study (Voet et al., 2025), we introduced a method to derive AoA from satellite-based measurements of SF_6 in combination with five long-lived trace gases: N_2O, CH_4, trichlorofluoromethane (CFC-11), CFC-12, and chlorodifluoromethane (HCFC-22). For this method — henceforth referred to as the multi-tracer method — an uncertainty-weighted mean AoA is derived from empirical relations between the five tracers and SF_6-based AoA. These empirical relations can be established directly from the satellite measurements without requiring any additional external information (Voet et al., 2025). In the previous study, we demonstrated a proof of concept for the multi-tracer method using noisy CLaMS-simulated tracer data rather than satellite observations. The derived relationships were also successfully applied to balloon-borne remote-sensing trace-gas measurements, indicating good performance with real observations.

In this study, we demonstrate the utility of the multi-tracer method relative to conventional approaches that rely on SF_6 alone, when applied to real satellite measurements. In addition to that, we introduce a new AoA product that can be used to study the long-term trends of the BDC, which are not yet fully understood. Although the method was originally developed for instruments with dense sampling (resulting in global coverage over a short period), such as the upcoming Stratosphere–Troposphere Response using Infrared Vertically-resolved light Explorer STRIVE (Jaeglé et al., 2025), we apply it here to the relatively sparse, but generally more precise, measurements from ACE-FTS, which provides the longest and most recent measurement record of all required trace gases.

The present study builds on Voet et al. (2025) and has two goals: (i) to provide a proof of concept specifically tailored to ACE-FTS measurements, and (ii) to investigate stratospheric circulation variability based on this new AoA product from ACE-FTS satellite data. For the first goal, output from a CLaMS simulation of the required trace gases and of the model's ideal clock tracer is interpolated to the locations and times of ACE-FTS observations. The typical measurement uncertainties of the tracers in the ACE-FTS dataset are then added as noise to the interpolated values, thereby creating synthetic measurements. AoA is then derived from these synthetic measurements of SF_6 alone (SF_6-only AoA) and from all six tracers combined (multi-tracer AoA), and both estimates are compared with the true AoA of the CLaMS model, as computed from its ideal clock tracer. For the second goal, multi-tracer AoA is derived from the actual ACE-FTS measurements over the full observation period, and its long-term trends are investigated and compared with the results of Dubé et al. (2025) and Saunders et al. (2025).

The structure of the study is as follows: the ACE-FTS instrument and the two dataset versions used are described in Sect. 2.1; the CLaMS model and its setup are presented in Sect. 2.2; the methods used to derive AoA from SF_6 alone and from the combination of all six trace gases are described in Sect. 2.3; the modifications applied to the ACE-FTS datasets to account for biases are outlined in Sect. 2.4; and the proof of concept based on the CLaMS model results is explained in Sect. 2.5. The results are presented and discussed in Sect. 3, including the proof of concept with synthetic measurements in Sect. 3.1, a comparison of climatologies of the two observational AoA estimates with each other and with model AoA in Sect. 3.2, a comparison of these estimates with AoA derived from in situ measurements in Sect. 3.3, and a trend analysis of the AoA

https://doi.org/10.5194/egusphere-2026-4647
Preprint. Discussion started: 2 September 2026

estimates, including a comparison with the results of Dubé et al. (2025) and Saunders et al. (2025), in Sect. 3.4. Section 4 presents the main conclusions drawn from the results and their discussion.

2 Methods

This section provides a detailed description of the methodology used in this study. Subsection 2.1 describes the ACE-FTS instrument and the datasets used, while Subsection 2.2 describes the CLaMS model and its setup. The two AoA estimation methods, based on SF_6 alone (convolution method) and on the combination of all six trace gases (multi-tracer method), are presented in Subsection 2.3. Subsection 2.4 briefly describes the prior preparation of SF_6 mixing ratios in the ACE-FTS datasets to account for a slight discrepancy relative to in situ surface measurements; Appendix A1 provides a more detailed account. Subsection 2.5 describes the proof of concept based on CLaMS model results.

2.1 ACE-FTS observations

The Atmospheric Chemistry Experiment – Fourier Transform Spectrometer (ACE-FTS; Bernath et al., 2005) is a high-spectral-resolution (0.02 cm^{-1}) infrared solar-occultation instrument aboard the Canadian SCISAT satellite, which has been operating since February 2004. During each sunrise and sunset occultation, ACE-FTS records atmospheric transmittance spectra in the range 750–4400 cm^{-1} using a Michelson interferometer (Boone et al., 2005). Volume mixing ratios (VMRs) of a large suite of trace gases are retrieved by fitting simulated spectra to these measurements (Boone et al., 2005). Each occultation provides a vertical profile with a resolution based on the field of view of about 3–4 km, reported on a 1 km grid, spanning altitudes typically between 6 and 150 km depending on the species. The effective resolution (oversampling effect at lower altitudes) is about 1.5 km. From its 74° orbital inclination, ACE-FTS achieves sampling up to 85° N/S, with approximately 30 occultations per day (two per orbit), with highest coverage at high latitudes. Global sampling is achieved over roughly three months, though measurements are not uniformly distributed in latitude or time.

Despite its relatively sparse sampling compared to other limb-viewing instruments like the Michelson Interferometer for Passive Atmospheric Sounding (MIPAS), or nadir-viewing instruments, ACE-FTS offers several advantages for stratospheric tracer studies. Its solar-occultation technique yields a high signal-to-noise ratio, essential for weak absorbers such as SF_6, which occurs at VMRs of only a few parts per trillion. The resulting 22-year, internally consistent record of long-lived trace gases — including SF_6, N_2O, CFC-11 (CCl_3F), CFC-12 (CCl_2F_2), HCFC-22 ($CHClF_2$), and CH_4 — is unique among available satellite datasets and provides a valuable basis for multi-tracer analyses of stratospheric transport.

In this study, we use the two ACE-FTS retrieval versions 3.6 and 5.2 for all six long-lived species. Version 3.6 employs the retrieval framework described by Boone et al. (2013) and corresponds to the v3.5/3.6 dataset analyzed by Saunders et al. (2025). Version 5.2 represents the processing release available through November 2024 and includes several major updates, including revised spectroscopic line parameters, optimized micro-window selection, and improved instrument line-shape characterization (Boone et al., 2023; Bernath et al., 2025). The latest processing release, version 5.3, is largely similar to version 5.2, with only

https://doi.org/10.5194/egusphere-2026-4647
Preprint. Discussion started: 2 September 2026

minor changes to the retrieval code and change in processing hardware. Version 5.2 was selected instead of 5.3 because the preprocessing required for version 5.3 was not yet completed at the time of writing.

However, as discussed by Saunders et al. (2025) and confirmed in this work, retrieval versions later than the v3 series (i.e., v4 and v5) can exhibit spurious features in SF_6 between approximately 18 and 30 km. This issue motivates a separate analysis of the two versions used in this study. All ACE-FTS data are accompanied by quality-control flags developed by Sheese et al. (2015). Following the recommended procedure, only measurements with a flag value of 0 were retained, and entire profiles were discarded if any level was flagged as 4 or 5. The temporal coverage of the datasets used here is 17 years (February 2004 to February 2021) for v3.6 and 19 years (December 2004 to December 2023) for v5.2. Detailed descriptions of the ACE-FTS instrument, retrieval algorithms, and version updates are provided by Bernath et al. (2005), Boone et al. (2013, 2020, 2023), and Saunders et al. (2025). Information on other satellite instruments within the WCRP SPARC Data Initiative is available in Tegtmeier et al. (2016), Hegglin and Tegtmeier (2017), and Hegglin et al. (2021).

2.2 Setup of the Chemical Lagrangian Model of the Stratosphere (CLaMS)

We employ the Chemical Lagrangian Model of the Stratosphere (McKenna et al., 2002b, a) in the version (CLaMS 2.0) and with the same configuration as described in detail by Voet et al. (2025). CLaMS is an offline Lagrangian chemical transport model that simulates the evolution of trace-gas mixing ratios along trajectories of individual air parcels. The Lagrangian representation allows the model grid to adapt dynamically in space and time, which facilitates the accurate treatment of small-scale mixing and transport processes.

The model is driven by meteorological fields from the European Centre for Medium- Range Weather Forecasts Reanalysis v5 (ERA5 Hersbach et al., 2023) and covers the period from 1 January 1979 to 31 December 2024. A 20-year spin-up simulation was performed using repeating 1979 meteorology and boundary conditions to ensure dynamically and chemically equilibrated initial conditions for the transient simulation. The model employs a hybrid vertical coordinate, ζ, that transitions from an orography-following coordinate in the troposphere to an isentropic coordinate in the stratosphere (Pommrich et al., 2014). The vertical grid consists of 45 layers, extending from the surface (ζ = 0 K) up to approximately the stratopause (about 55 km, or 2350–2650 K).

Six trace gases with long stratospheric lifetimes are included in the model: SF_6, CFC-11, CFC-12, HCFC-22, CH_4, and N_2O. Zonal-mean surface time series of these species based on observations by the Global Monitoring Laboratory (GML) of the National Oceanic and Atmospheric Administration (NOAA) provide the lower boundary conditions (Dutton et al., 2026a; Lan et al., 2024c, b; Dutton et al., 2026b, c; Montzka et al., 2015; NOAA Global Monitoring Laboratory, 2026; Lan et al., 2024a). Upper boundary conditions are tracer-specific: SF_6 is constrained by monthly zonal-mean time series derived from measurements by the Michelson Interferometer for Passive Atmospheric Sounding (MIPAS; Fischer et al., 2008; Kiefer, 2021) that operated on the ESA Environmental Satellite (Envisat); for CH_4 boundary conditions are based on the climatology of the Halogen Occultation Experiment (HALOE, Grooß and Russell, 2005); for N_2O on the Mainz photochemical 2-D model (Grooß, 1996), CFC-11, and CFC-12 are set to zero at the uppermost layer, consistent with their complete destruction in the stratosphere. For HCFC-22, an open (zero-flux) upper boundary is applied. In addition, an ideal “clock tracer”, i.e a passive

https://doi.org/10.5194/egusphere-2026-4647
Preprint. Discussion started: 2 September 2026

trace gas with a linearly increasing surface mixing ratio, is included to determine the actual mean age of air of the model environment (c.f. Hall and Plumb, 1994). For more details about the creation of the boundary conditions see Voet et al. (2025)

The vertical cross-isentropic transport is derived from ERA5 diabatic heating rates following Ploeger et al. (2021). Convection is parameterized using convective available potential energy (CAPE) as a trigger for unresolved convection (Konopka et al., 2019), consistent with the CLaMS configuration used by Konopka et al. (2022). Further details on the model setup, chemical loss schemes, and validation against observations are provided by Voet et al. (2025).

2.3 Age of air calculation

The convolution method described by Garny et al. (2024b) provides the foundation for the AoA analysis in this study. The underlying formulation, originally introduced by Hall and Plumb (1994), relates the observed mixing ratio μ_{obs} of a passive tracer (without sources or sinks outside the boundary region) at the observation point P_{obs} and time t_{obs} to the history of tracer mixing ratios at the boundary region, $\mu_{\text{ref}}(t)$, via the age-of-air spectrum $\mathcal{G}(t, t_{\text{obs}})$. The latter represents the distribution of transit times of individual air parcels arriving at P_{obs} at time t_{obs} that originated in the boundary region:

$$\mu_{\text{obs}} = \int_0^\infty \mu_{\text{ref}}(t - t_{\text{obs}})\, \mathcal{G}(t, t_{\text{obs}})\, \mathrm{d}t. \tag{1}$$

Note that, for simplicity, the dependence of $\mathcal{G}$ on P_{obs} is not explicitly stated in the relation above. Hall and Plumb (1994) demonstrated that the inverse Gaussian distribution

$$G(\Gamma, \Delta, \tau) = \sqrt{\frac{\Gamma^3}{4\pi\Delta^2\tau^3}} \exp\left(-\frac{\Gamma(\tau - \Gamma)^2}{4\Delta^2\tau}\right), \tag{2}$$

fully parameterized by its first moment Γ and its width Δ (square root of second central moment divided by two), can be used as an approximation of the age spectrum $\mathcal{G}$ in the stratosphere. They further showed that the ratio $\frac{\Delta^2}{\Gamma}$, often referred to as the ratio of moments (RoM), remains approximately constant throughout the stratosphere, although more recent work has shown that this can be a rather crude approximations (Hauck et al., 2020). In the convolution framework of Garny et al. (2024b), the age spectrum at a given observation point is represented by an inverse Gaussian distribution with a constant ratio of moments. This ratio can be estimated from model simulations, and may in principle also be constrained by observations. The spectrum $G(\Gamma, \Delta, \tau)$ is then evaluated numerically across a wide range of possible Γ values, with the convolution solved for each case. The value of Γ that best reproduces the observed tracer mixing ratio μ_{obs} is taken as the mean age of air at the point and time of observation.

In their study, Garny et al. (2024b) used CO_2 and SF_6 — the most widely employed tracers for deriving the mean age of air — as approximations for the passive tracer μ. Their analysis relied on climatological mean values of $\frac{\Delta^2}{\Gamma}$ derived from CLaMS simulations, driven by the ERA-Interim reanalysis. At the time, this ratio of moments was largely unconstrained by observations, making model-based estimates a pragmatic choice. Although more recent observational analyses by Ray et al. (2024) have better constrained the ratio of moments, their results remain broadly consistent with model-based estimates and

https://doi.org/10.5194/egusphere-2026-4647
Preprint. Discussion started: 2 September 2026

are primarily presented as a validation of the latter rather than a replacement for further applications. As the boundary reference time series $SF_{6,\mathrm{ref}}(t)$, Garny et al. (2024b) used monthly mean values from Cape Grim, Tasmania (adjusted to tropical latitudes up to 1995), and NOAA Marine Boundary Layer data for the tropics. Saunders et al. (2025) applied the convolution method based on SF_6, using the identical $\frac{\Delta^2}{\Gamma}$ climatology and reference time series $SF_{6,\mathrm{ref}}(t)$ as Garny et al. (2024b). However, they found that, over time, SF_6 mixing ratios in the ACE-FTS dataset version 3.6 at tropical latitudes and tropospheric altitudes tended to fall slightly below the corresponding values in the reference time series $SF_{6,\mathrm{ref}}(t)$. To account for this bias, Saunders et al. (2025) derived correction factors by fitting a third-order polynomial via least squares to the relative differences between the reference and measured values. The bias was then corrected by multiplying all SF_6 values in dataset with the corresponding time-dependent correction factor.

The present study employs the same $\frac{\Delta^2}{\Gamma}$ climatology and reference time series $SF_{6,\mathrm{ref}}(t)$ as Saunders et al. (2025). In a first step, mean age of air is derived from SF_6 for the ACE-FTS datasets (versions 3.6 and 5.2) at each observation point over the full temporal coverage of the datasets. These SF_6-based AoA estimates are subject to considerable uncertainty, primarily because of the challenges associated with retrieving SF_6 from ACE-FTS measurements (Boone et al., 2005, 2013, 2020, 2023). To reduce this uncertainty, in a second step we applied a refined version of our original multi-tracer method (Voet et al., 2025). This method exploits strong and compact correlations between other long-lived trace gases and AoA to estimate a set of new AoA values, which are then used in combination to replace the initial first guess derived solely from SF_6. Voet et al. (2025) established the correlations based on model results as a proof of concept, but also showed that fully observation-based correlations can be obtained from an "a-priori" SF_6-based AoA, for example calculated from the convolution method described therein.

As ACE-FTS measurements are comparatively sparse, the required correlations can only be established over periods of several days to weeks rather than on a single day. Instead of geographic latitude, equivalent latitude based on ERA5 reanalysis data was used to assign the observed points over the considered period to different geographical regions. In addition, we subdivided the global equivalent latitude range into five regions rather than considering only the two hemispheres: the southern polar (90°S–60°S), southern mid-latitudes (60°S–30°S), tropics (30°S–30°N), northern mid-latitudes (30°N–60°N), and the northern polar (65°N–90°N). Note that the different latitudinal boundaries for the southern and northern polar regions approximate the climatological stratospheric polar vortex edge in the two hemispheres. This approach better accounts for the dynamical characteristics of different air masses. For each day in the measurement periods of the two ACE-FTS datasets, all observed points within a 15-day window — spanning seven days before to seven days after the given day — were assigned to the five regions above based on equivalent latitude.

We selected the same additional five long-lived trace gases as in Voet et al. (2025): N_2O, CH_4, CFC-11, CFC-12, and HCFC-22. These five trace gases are reliably retrieved from the transmittance spectra observed by ACE-FTS and their long atmospheric lifetimes (see e.g. Vervalcke et al., 2026) guarantee at least partially tight correlations with AoA. To obtain compact correlations, only data below an altitude of 30 km were used, with tracer mixing ratios plotted against SF_6-derived AoA for each latitude region. For each correlation, we constructed a lookup table linking tracer mixing ratios to AoA values. Unlike the original study, where the data were first binned by mixing ratio and the midpoint of the bins were smoothed with a Savitzky–Golay filter,

https://doi.org/10.5194/egusphere-2026-4647
Preprint. Discussion started: 2 September 2026

we generated smoothed lookup tables using Gaussian Process Regression (GPR) with the `GaussianProcessRegressor` model and the `RBF` and `WhiteKernel` kernels from the `sklearn.gaussian_process` library (Pedregosa et al., 2011). This approach has the advantage that no prior subdivision of the data into arbitrary mixing ratio bins or zonal averaging of the data is required. The regression was performed in two iterations. In the first iteration, all data points were included, while in the second only those within twice the predicted standard deviation of the first iteration's AoA were retained, thereby excluding outliers.

The predicted values from the second iteration form lookup tables (LUTs) that map a given mixing ratio within the correlation range to the corresponding AoA and uncertainty ΔAoA. These values are obtained by linear interpolation for the mixing ratio in question. A small correction was applied to the lookup tables to avoid overestimated AoA values at the upper end of the mixing ratio scale (see Sect. B in the appendix for details). Figure C1 in the appendix shows the final lookup tables for the five trace gases in the 30°S–30°N equivalent-latitude band on 11 November 2011 as an example.

For each ACE-FTS observation below 30 km in the two dataset versions (3.6 and 5.2), an AoA value AoA_i with uncertainty σ_i was derived for each selected tracer i, using the corresponding lookup table for the day of observation, equivalent latitude band, and dataset version. From the five AoA estimates at each observation point, an uncertainty-weighted mean value

$$\overline{\mathrm{AoA}} = \frac{\sum_i \left(\sigma_i^{-2}\,\mathrm{AoA}_i\right)}{\sum_i \sigma_i^{-2}} \tag{3}$$

and the corresponding uncertainty

$$\overline{\sigma} = \sqrt{\frac{1}{\sum_i \sigma_i^{-2}}} \tag{4}$$

were calculated, following Voet et al. (2025). After this step, the method of Garny et al. (2024a) was applied to $\overline{\mathrm{AoA}}$ to correct for the influence of SF_6-depleted air transported downward from the mesosphere. From here on, the method described above to derive an uncertainty-weighted mean AoA from multiple trace gases and correct it for the mesospheric sink of SF_6 will be referred to as the multi-tracer method, and the corresponding AoA values will be called multi-tracer AoA. Similarly, the convolution method described at the beginning of this subsection, applied to SF_6 mixing ratios in combination with the mesospheric sink correction, will be referred to as the SF_6-only method, and the corresponding AoA values will be called SF_6-only AoA.

Multi-tracer AoA values and SF_6 mixing ratios at individual observation points in the two datasets were sampled into 10°latitude bins from 90°S to 90°N, consistent with Saunders et al. (2025), below 30 km for the 1-month, 3-month, and 2004–2021 time periods. Zonal-mean values and standard deviations were then calculated from the sampled datasets. The SF_6-only method was applied to the zonal-mean SF_6 mixing ratios as well as to those values plus and minus their standard deviations, to derive zonal-mean SF_6-only AoA with uncertainty estimates free of high-value bias (see Section B).

https://doi.org/10.5194/egusphere-2026-4647
Preprint. Discussion started: 2 September 2026

2.4 Accounting for biases in SF_6 mixing ratios of ACE-FTS dataset version 3.6 and 5.2

A bias in SF_6 mixing ratios directly translates into a bias in the derived AoA if left uncorrected. Saunders et al. (2025) investigated a potential bias in SF_6 in the ACE-FTS version 3.6 dataset by constructing a time series of monthly zonal-mean SF_6 mixing ratios at tropical latitudes (17.5°S–17.5°N) and tropospheric altitudes (at least 2 km below the tropopause, as defined by the World Meteorological Organization, WMO), and comparing it with the reference time series $SF_{6,\mathrm{ref}}(t)$. They found that the ACE-FTS measurements initially agreed well with the reference values but gradually drifted toward lower values from around 2014 onward. To correct for this drift, Saunders et al. (2025) applied correction factors to the ACE-FTS SF_6 data, derived from a polynomial least-squares fit to the relative differences between the two time series. In the present study, the correction was carried out in a similar manner, but with the least-squares fit performed on the absolute differences between the two time series, and the relative differences calculated afterward from the fit results and the reference time series $SF_{6,\mathrm{ref}}(t)$. A detailed description of the applied correction method is given in Appendix A1.

2.5 Proof of concept using the Chemical Lagrangian Model of the Stratosphere (CLaMS)

In the first step of the study, a proof-of-concept of the multi-tracer method to calculate AoA from ACE-FTS measurements is carried out in a "clean" model environment where both the "observable" trace gas species as well as the resulting mean age are known. The model tracers interpolated to the ACE-FTS measurement locations using a trajectory mapping technique (cf. Ploeger et al., 2013) were used to generate synthetic or simulated measurements for testing the multi-tracer method described in Sect. 2.3 for both ACE-FTS dataset versions (v3.6 and 5.2). Therefore, normally distributed random noise was added to the model-based tracer mixing ratios, based on empirical standard deviations calculated from the measurement data. Note that a sensitivity calculation with the published ACE-FTS tracer uncertainties interpreted as the standard deviations resulted in an excessive spread. Hence, the here used standard deviations for generating synthetic measurements reflect not only measurement uncertainty but also natural variability. Since the interpolated model-based mixing ratios already account for the model-estimated natural variability, adding random noise based on the empirical standard deviations directly would result in a more excessive spread. To address this, the model-estimated natural variability was removed before the random noise was added, by averaging the model-based data over the corresponding regions and time periods. The synthetic measurements were calculated as follows. For each year, the data were divided into non-overlapping 15-day periods and 10° equivalent latitude bins from 90°S to 90°N. Within each period, bin, and height level, empirical standard deviations were calculated from the measurement, while mean values were calculated from the model data of each trace gas. Due to data sparsity in some subsets, the empirical standard deviations were subsequently averaged over the entire year for each latitude bin and height level. Using these annual average standard deviations, normally distributed random noise was generated and added to the model-based mean values at the corresponding latitude bin and height level for each 15-day period.

For the proof of concept, the synthetic measurements were processed in the same way as the actual observations using the procedure described in Section 2.3, with three modifications to the calculation of AoA from SF_6. First, instead of the reference time series recommended by Garny et al. (2024b), AoA from synthetic SF_6 was calculated using the model's lower-boundary

https://doi.org/10.5194/egusphere-2026-4647
Preprint. Discussion started: 2 September 2026

mixing ratio time series averaged from 30°S to 30°N. Second, to maintain consistency with the CLaMS setup used in this study, climatological mean values of the ratio of moments $\frac{\Delta^2}{\Gamma}$ derived from ERA5-driven CLaMS were used rather than those from ERA-Interim, which were suggested by Garny et al. (2024b) and used for the actual ACE-FTS observations in this study. Third, the correction for mesospheric SF_6-depleted air was adapted: because the ERA5 stratospheric circulation has been shown to be somewhat slow-biased compared with observations (Laube et al., 2020; Ploeger et al., 2021), the parameters of the correction method of Garny et al. (2024a) were recalculated for the ERA5-driven CLaMS SF_6. These three adjustments ensure the most accurate possible calculation of SF_6-derived AoA in the model environment.

Figure C2 in the appendix illustrates the lookup tables for the same cases as in Figure C1, but derived from synthetic SF_6-based AoA and tracer mixing ratios. The spread of the points is comparable between the two figures. This close agreement in data spread between synthetic and actual measurements was found consistently across all cases, not only in the example shown.

Zonal-mean values and standard deviations for the SF_6-only and multi-tracer AoA values derived from the synthetic measurements for the two dataset versions were calculated in the same way as the corresponding AoA values derived from the actual measurements (see the end of Sect. 2.3). For comparison, the actual AoA values of the CLaMS model environment, derived from its ideal clock tracer, were also interpolated to the observation points of the two datasets. Zonal-mean values for this CLaMS model AoA were calculated in the same way as for the AoA values derived from the synthetic measurements.

3 Results

We conducted an extensive analysis comparing the ACE-FTS datasets (v3.6 and v5.2) and the two AoA calculation methods (SF_6-only and multi-tracer). The results are presented in the following subsections: 1) a proof of concept within the CLaMS model (Sect. 3.1), 2) the mean state of the stratospheric circulation (Sect. 3.2), 3) validation against in situ measurements (Sect. 3.3), and 4) multidecadal trends over the satellite observation period (Sect. 3.4). For the proof of concept, both AoA methods were applied to simulated ACE-FTS datasets based on CLaMS model output (see Sect. 2.5), while the actual ACE-FTS datasets were used in all subsequent subsections (Sect. 3.2 to Sect. 3.4). Given the shorter observation period and higher sparsity of version 3.6 compared with version 5.2, we present version 5.2 in the proof of concept in Sect. 3.1 and the trend analysis in Sect. 3.4 and provide the corresponding version 3.6 results in the Appendix where necessary.

3.1 Proof of concept for the multi-tracer method

For the proof of concept, zonal-mean values averaged over 3-month periods are considered, as it takes roughly 3 months for the ACE-FTS measurements to achieve global coverage. Furthermore, the tracer-based AoA estimates in this section, SF_6-only AoA and multi-tracer AoA, are derived exclusively from synthetic measurements generated from the CLaMS model, as described in Sect. 2.5.

Figure 1 shows the zonal-mean values for SF_6-only AoA and multi-tracer AoA for dataset version 5.2 for the periods December 2011–February 2012 and June–August 2012. The corresponding zonal-mean AoA values from the ideal clock

https://doi.org/10.5194/egusphere-2026-4647
Preprint. Discussion started: 2 September 2026

tracer of the CLaMS model are also shown. SF_6-only AoA (panels c, f) exhibits substantial noise due to the high measurement uncertainty of SF_6, which is significantly reduced in the multi-tracer AoA (panels a, d).

The general structure of the true AoA distributions (panels b, e) — with younger air at lower altitudes and latitudes — remains recognizable in the SF_6-only AoA (panels c, f), but the overall agreement between the two is poor. Multi-tracer AoA (panels a, d) shows much closer agreement with the true AoA distributions for both seasons.

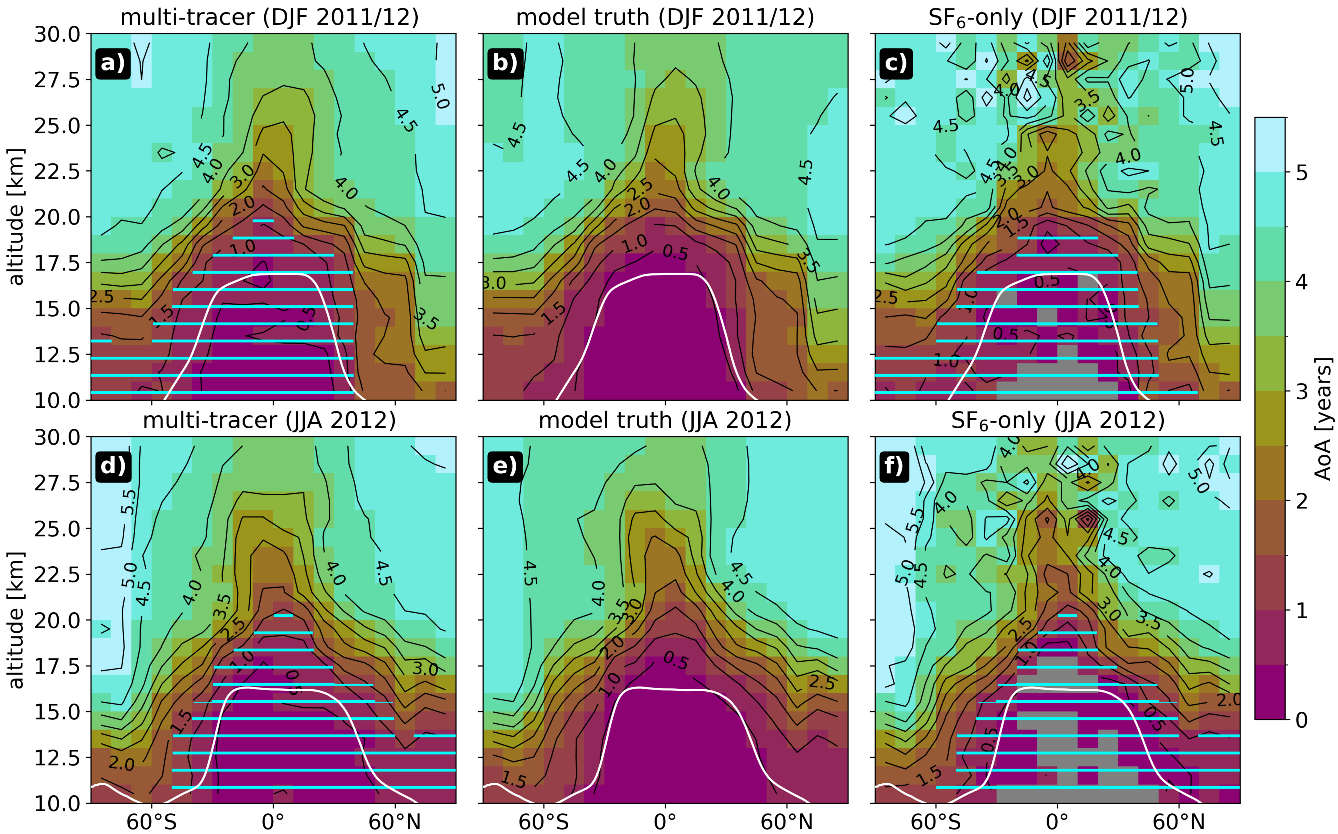

Figure 1. Zonal-mean AoA over three-month periods based on CLaMS model results interpolated onto ACE-FTS dataset version 5. Upper panels (a–c): December 2010–February 2011. Lower panels (d–f): June–August 2011. (a, d): AoA derived from the combination of six long-lived trace gases. (b, e): Actual AoA of the model environment. (c, f): AoA derived using the convolution method with SF_6 only. Thick white lines: Mean tropopause height based on ERA5 reanalysis. See Sections 2.3 and 2.5 for details. Blue hatched regions: areas around the tropopause with tracer-based AoA below 1.5 years.

To further demonstrate the advantages of the multi-tracer method, we quantified the accuracy (systematic uncertainty) and precision (statistical uncertainty) of the two AoA calculation methods. Accuracy was defined as the difference between the zonal mean of each tracer-based AoA estimate and the model's true AoA. Precision was estimated as the standard deviation of these differences across longitudes. Specifically, differences between each tracer-based AoA estimate and the model's true

https://doi.org/10.5194/egusphere-2026-4647
Preprint. Discussion started: 2 September 2026

AoA were computed at every observation point, then grouped into latitude–altitude bins for each 3-month period following the procedure described at the end of Sect. 2.3. The standard deviation was calculated for each bin.

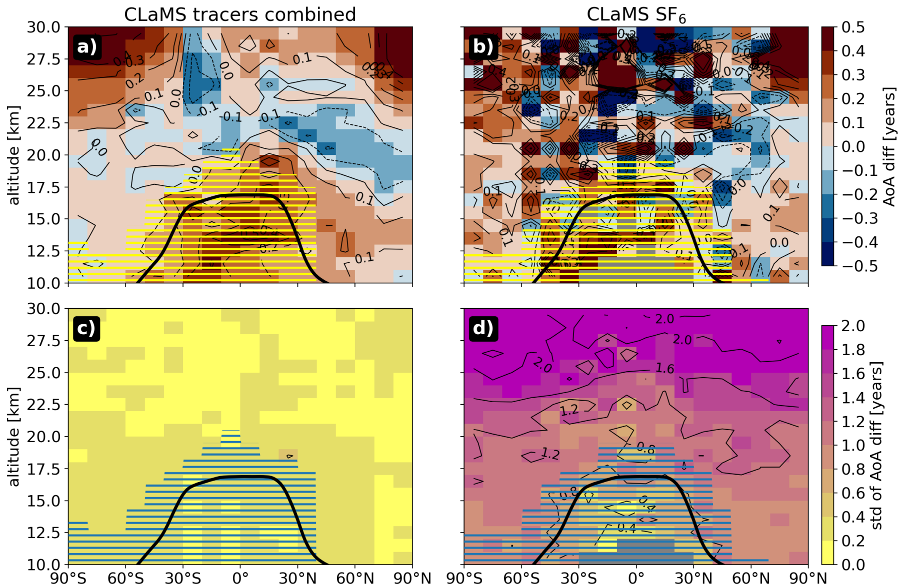

Figure 2. Mean values and standard deviations of the differences between CLaMS-tracer-based AoA estimates and the model's true AoA in the zonal direction for dataset version 5.2 for December 2011–February 2012. (a, c): multi-tracer AoA. (b, d): SF_6-only AoA. (a) Zonal-mean differences. (b) Differences of zonal means (first zonally averaged than subtracted to avoid bias caused by missing would-be negative values; see introduction to Section 2). (c, d) Standard deviations of the zonal differences. Thick black lines: mean tropopause height from ERA5 reanalysis. Hatched regions: areas around the tropopause with tracer-based AoA below 1.5 years (yellow hatching in panels a,b; blue hatching in panels c,d).

Figure 2 shows the zonal means and standard deviations for dataset version 5.2 for the period December 2011–February 2012. The substantial noise in SF_6-only AoA, visible in panel c of Figure 1, is also reflected in the corresponding zonal-mean differences in panel b of Figure 2. Larger contiguous regions where the SF_6-only AoA agrees with the model's true AoA within approximately ±0.3 years are found only at higher latitudes below 25 km, particularly in the Northern Hemisphere. In contrast, zonal-mean differences for multi-tracer AoA (panel a of Figure 2) show far less noise, and contiguous regions of agreement within ±0.3 years can be found throughout the stratosphere. Both synthetic tracer-based AoA estimates are noticeably older than the true AoA of the model in the polar regions at high altitudes. These overestimations are likely caused by an insufficient correction for SF_6-depleted air transported downward from the mesosphere for the air masses with particularly high level of SF_6 depletion encountered there. For simplicity, the parameters of the SF_6 sink correction are calculated as global averages and therefore do not fully correct for SF_6 depletion in especially old air masses (e.g. Garny et al., 2024a).

On average, the absolute difference amounts to roughly 0.14 years for the multi-tracer AoA (panel a) and 0.26 years for the SF_6-only AoA (panel b) above the 1.5-year threshold, but with strong variability for the latter. Using multiple trace gases

https://doi.org/10.5194/egusphere-2026-4647
Preprint. Discussion started: 2 September 2026

therefore improves the accuracy of the estimated zonal-mean AoA by almost 50%. The standard deviations in panel d of Figure 2 indicate a substantial spread of SF_6-only AoA around the model's true AoA, from roughly 0.8 years at lower altitudes to over 2 years at the upper end of the altitude range. Note that these standard deviations might be biased because negative AoA values are not defined, which introduces a high bias when AoA derived with the convolution method is averaged (see Sect. B); caution is therefore warranted. In contrast, the standard deviations for multi-tracer AoA are evenly distributed across the altitude range and amount to roughly 0.21 years. The total uncertainty of a derived AoA value at a single observation point can be estimated as the root mean square of the corresponding mean difference and standard deviation at the given latitude and altitude. Combining the mean differences and standard deviations in this way yields an average of ∼0.3 years for the multi-tracer AoA at any latitude and altitude, indicating the potential usefulness of the multi-tracer method even for individual measurement profiles. By contrast, the average total uncertainty for the SF_6-only AoA amounts to ∼1.6 years.

Figure D2 in the Appendix shows the corresponding situation to Figure 2, but for the period June–August 2011. The results in the two figures are very similar, with the reversal of the winter and summer hemispheres leading to corresponding reversals in the regions of higher uncertainty. The results in Figures 1, 2, and D2 are consistent for both ACE-FTS dataset versions and for all analyzed 3-month periods throughout the full temporal coverage of the datasets.

3.2 Climatological state of the stratospheric circulation

From here onward, the tracer-based AoA estimates, i.e., SF_6-only AoA and multi-tracer AoA, are derived exclusively from the actual ACE-FTS measurements. AoA estimates based on synthetic measurements generated with the CLaMS model, as described in Sect. 2.5, are presented only in Sect. 3.1.

Figure 3 shows the zonal-mean multi-tracer AoA and zonal-mean SF_6-only AoA for dataset version 3.6 and 5.2 over the period from 2004 to 2021 (Full period coverd by version 3.6). The light-blue hatched regions around the tropopause indicate young air masses with mean ages below 1.5 years. For these values, it cannot be ruled out that the air has been influenced by tropospheric transport from extratropical regions, so the single-entry-point assumption required for the calculation of stratospheric mean age of air may no longer hold. Caution is therefore warranted when interpreting these values.

The SF_6-only AoA distribution for dataset version 5.2 (panel d) differs notably from the others: A secondary maximum in AoA in the lower stratosphere across all latitudes (around 20-22 km in the extratropics and 22-24 km in the tropics). Saunders et al. (2025) noted similar behaviour for ACE-FTS dataset version 4.1. This feature is most likely caused by updates to the retrieval algorithm in datasets after version 3.6. In the multi-tracer AoA distribution, however, the secondary maximum is almost completely resolved, possibly indicating that information from the additional long-lived trace gases corrects a systematic error in the SF_6 retrieval. Note that in Fig. 1, there is no such secondary maximum in the multi-tracer AoA derived from the synthetic measurements of dataset version 5.2, as the synthetic measurements are based on CLaMS model results and not on a retrieval of tracer mixing ratios from actual measurements (for further details see Sect. 2.5). For dataset version 3.6, the general shapes of the two AoA distributions agree well. Nevertheless, the multi-tracer AoA (panel a) is overall smoother than the SF_6-only AoA (panel c), and in the tropics the SF_6-only AoA is noticeably younger than the multi-tracer AoA. Relative to version 3.6, dataset version 5.2 shows lower AoA above roughly 20 km and higher or similar AoA below 20 km.

https://doi.org/10.5194/egusphere-2026-4647
Preprint. Discussion started: 2 September 2026

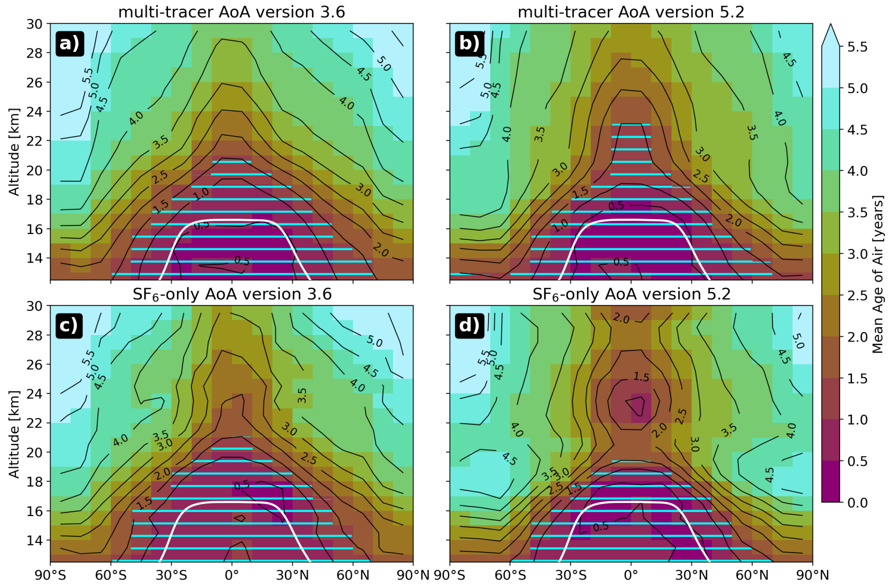

Figure 3. Zonal-mean AoA estimates from ACE-FTS measurements over the period 2004 to 2021 ACE-FTS. Left panels (a, c): version 3.6. Right panels (b, d): version 5.2. Upper panels (a, b): multi-tracer AoA. Lower panels (c, d): SF_6-only AoA. Thick white lines: mean tropopause height from ERA5 reanalysis. Hatched regions (blue lines): values below 1.5 years near the tropopause.

Figure 4 shows the differences between the zonal-mean ACE-FTS-based AoA estimates in Fig. 3 and the corresponding zonal-mean CLaMS model AoA over the same period. All four ACE-FTS-based AoA estimates are younger than the ERA5-driven CLaMS model AoA over most of the stratosphere, as indicated by the fact regions with negative values are larger than regions with positive values in all panels of Fig. 4. The generally higher CLaMS model AoA reflects the fact that the BDC is too slow in the ERA5 reanalysis dataset used to drive the CLaMS simulation (see e.g. Laube et al., 2020; Ploeger et al., 2021). However, in two regions the ACE-FTS-based AoA estimates exceed the CLaMS model AoA. The first region is located in the lower stratosphere near the tropopause. For dataset version 3.6, the multi-tracer and SF_6-only AoA fall almost entirely below 1.5 years in this region; therefore, the conditions required for the calculation of stratospheric mean age of air cannot be guaranteed. Because of the secondary AoA maximum in dataset version 5.2, especially for SF_6-only AoA, this first region extends farther into the lower stratosphere in version 5.2 than in version 3.6. The secondary AoA maximum in dataset version 5.2 is clearly visible in the illustrated differences, which further suggests that it is likely caused by an artefact of the updated retrieval algorithm. The other region where the ACE-FTS-based AoA estimates exceed the CLaMS model AoA is located at high latitudes and altitudes, especially the polar regions above roughly 24 km in both hemispheres. Similar to the situation for the synthetic tracer-based AoA estimates in Fig. 2 of Sect. 3.1, the ACE-FTS-based AoA estimates exceed the CLaMS model AoA values in this region because of the insufficient correction for SF_6-depleted air for air masses with particularly high levels of depletion.

https://doi.org/10.5194/egusphere-2026-4647
Preprint. Discussion started: 2 September 2026

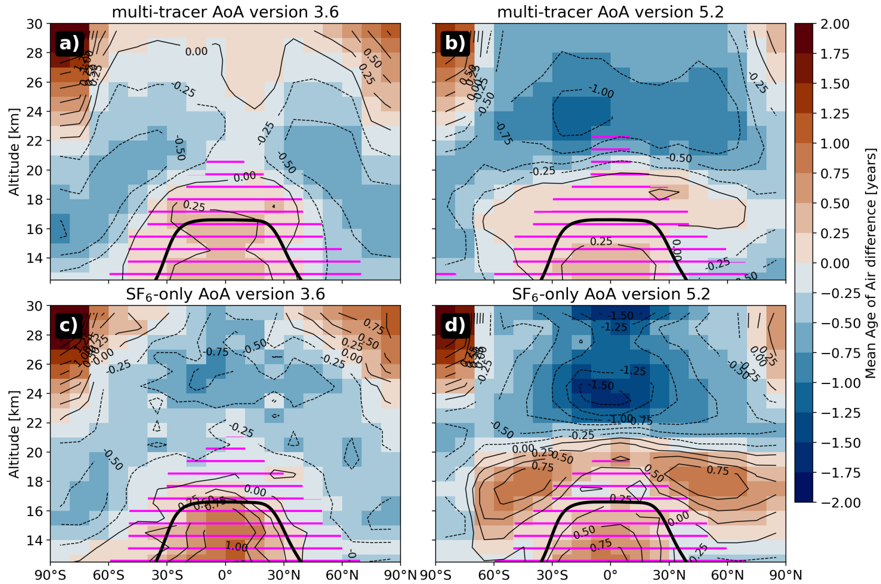

Figure 4. Zonal-mean AoA estimates from ACE-FTS measurements minus CLaMS model AoA over the period 2004 to 2021. Left panels (a, c): version 3.6. Right panels (b, d): version 5.2. Upper panels (a, b): multi-tracer AoA. Lower panels (c, d): SF_6-only AoA. Thick black lines: mean tropopause height from ERA5 reanalysis. Hatched regions (magenta lines): region near the tropopause where AoA estimate from ACE-FTS falls below 1.5 years.

Figure 5 shows examples of zonal-mean values over two specific 3-month periods, December 2011–February 2012 and June–August 2012, for dataset version 5.2 and both AoA types. In both seasons, the SF_6-only AoA (panels b, d) exhibits substantial noise due to the high measurement uncertainty of SF_6 and the relatively small number of data points compared with the full measurement period (panel d of Fig. 3). By contrast, the multi-tracer AoA (panels a, c) appears much smoother in both cases. The corresponding results for dataset version 3.6 (Fig. D1 in the Appendix) show a similar reduction in noise for the multi-tracer AoA. The larger data gaps (gray areas) in Fig. D1 compared with Fig. 5 result from the greater number of missing values in version 3.6 than in version 5.2.

https://doi.org/10.5194/egusphere-2026-4647
Preprint. Discussion started: 2 September 2026

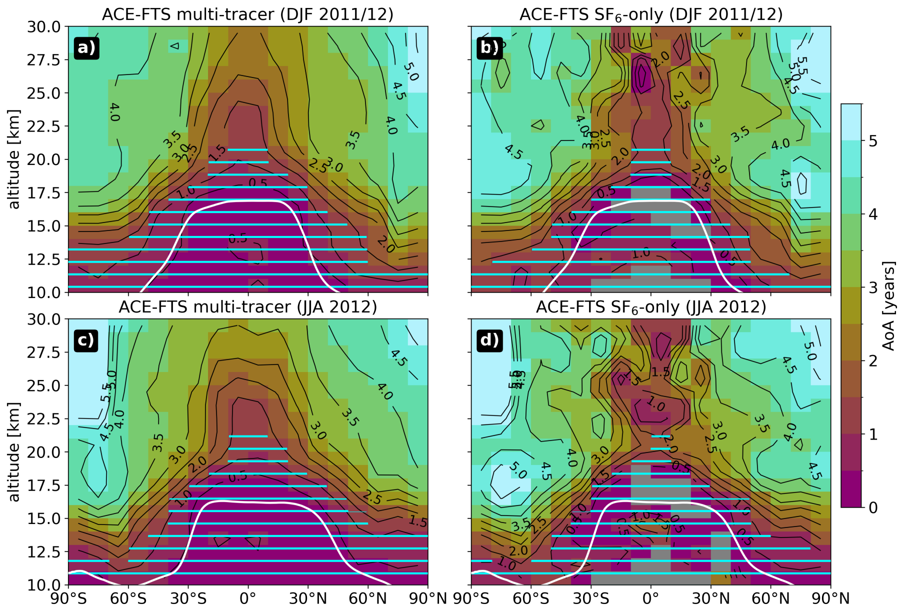

Figure 5. Zonal-mean AoA over three-month periods based on ACE-FTS dataset version 5.2. Upper panels (a–b): December 2011–February 2012. Lower panels (c–d): June–August 2012. (a, c): multi-tracer AoA. (b, d): SF_6-only AoA. Thick white lines: Mean tropopause height based on ERA5 reanalysis. Hatched regions (blue lines): values below 1.5 years near the tropopause. See Sections 2.3 for details. Gray areas: Missing values due to lack of data.

https://doi.org/10.5194/egusphere-2026-4647
Preprint. Discussion started: 2 September 2026

3.3 Comparison with in situ measurements

The aim of comparing AoA estimates from in situ measurements with those derived from ACE-FTS measurements is to assess which dataset version and which AoA estimation method is more reliable. For this purpose, we compared the AoA estimates derived from ACE-FTS measurements with the compiled dataset of estimated zonal-mean vertical and horizontal AoA profiles published by Garny et al. (2024c) as well as with AoA derived from SF_6 measured during individual aircraft campaigns and balloon launches.

The AoA values in the compiled dataset were derived from in situ measurements of SF_6 and CO_2 mixing ratios obtained during a variety of aircraft campaigns and balloon launches conducted between 1975 and 2023. The dataset includes vertical AoA profiles for the latitude bands 30°S–30°N (tropical latitudes), 30°N–60°N (northern midlatitudes), and 60°N–90°N (northern high latitudes), as well as a horizontal AoA profile at 20 km altitude. Vertical profiles of the multi-tracer AoA and SF_6 mixing ratios from the two ACE-FTS datasets were sampled within the corresponding three latitude bands over the full observation periods, and within 10° latitude bins across the full latitude range at 20±1 km altitude over the same periods. The resulting samples were used to calculate means and standard deviations. Upper and lower estimates of the mean ACE-FTS SF_6 profiles were obtained by adding and subtracting the standard-deviation profiles. SF_6-only AoA profiles, including upper and lower bounds, were then derived from these mean SF_6 profiles and their limits for both datasets using the convolution method and sink correction.

The aircraft campaigns were carried out with the Geophysica high-altitude aircraft between 2009 and 2017 over a broad latitude range in the Northern Hemisphere; campaign details are listed in Table 1. Balloon launches were conducted between March and October 2018 from Norwich, England (52.4°N). The balloon-borne measurements were made with AirCores, and flight details are listed in Table 2. AoA values were derived from these in situ SF_6 measurements using the convolution method followed by sink correction (see Sect. 2.3). For each aircraft campaign and each pair of balloon launches in the same season, vertical profiles of SF_6 mixing ratios and the corresponding multi-tracer AoA values from ACE-FTS dataset versions 3.6 and 5.2 were sampled within ±20 days of the mean observation time and within ±7.5°of the mean flight latitude. The relatively large temporal and latitudinal ranges were chosen to ensure a sufficient number of sampled profiles given the sparse ACE-FTS observations. Mean multi-tracer AoA and SF_6-only AoA profiles, together with uncertainty ranges, were calculated from these samples in the same way as for the compiled dataset.

Figure 6 presents the AoA profiles of the compiled dataset together with the corresponding ACE-FTS-based estimates. Figures 7 and 8 show the respective AoA profiles for the aircraft campaigns and balloon launches. A few general remarks can be made for the all three figures. Similar to the results in the previous two sections, the multi-tracer AoA profiles appear smoother and less affected by noise than the SF_6-only AoA profiles, with the estimated uncertainty ranges, that is, the spread within the sample, being significantly smaller for the former than for the latter. This reduced spread and smoother shape are especially evident for the comparisons to the aircraft campaigns and balloon launches, where fewer ACE-FTS profiles were averaged compared to the compiled dataset. Two other features noted in the previous sections are also apparent. The first is the secondary AoA maximum of the SF_6-only AoA in dataset version 5.2 around 20 km, where AoA begins to decrease with

https://doi.org/10.5194/egusphere-2026-4647
Preprint. Discussion started: 2 September 2026

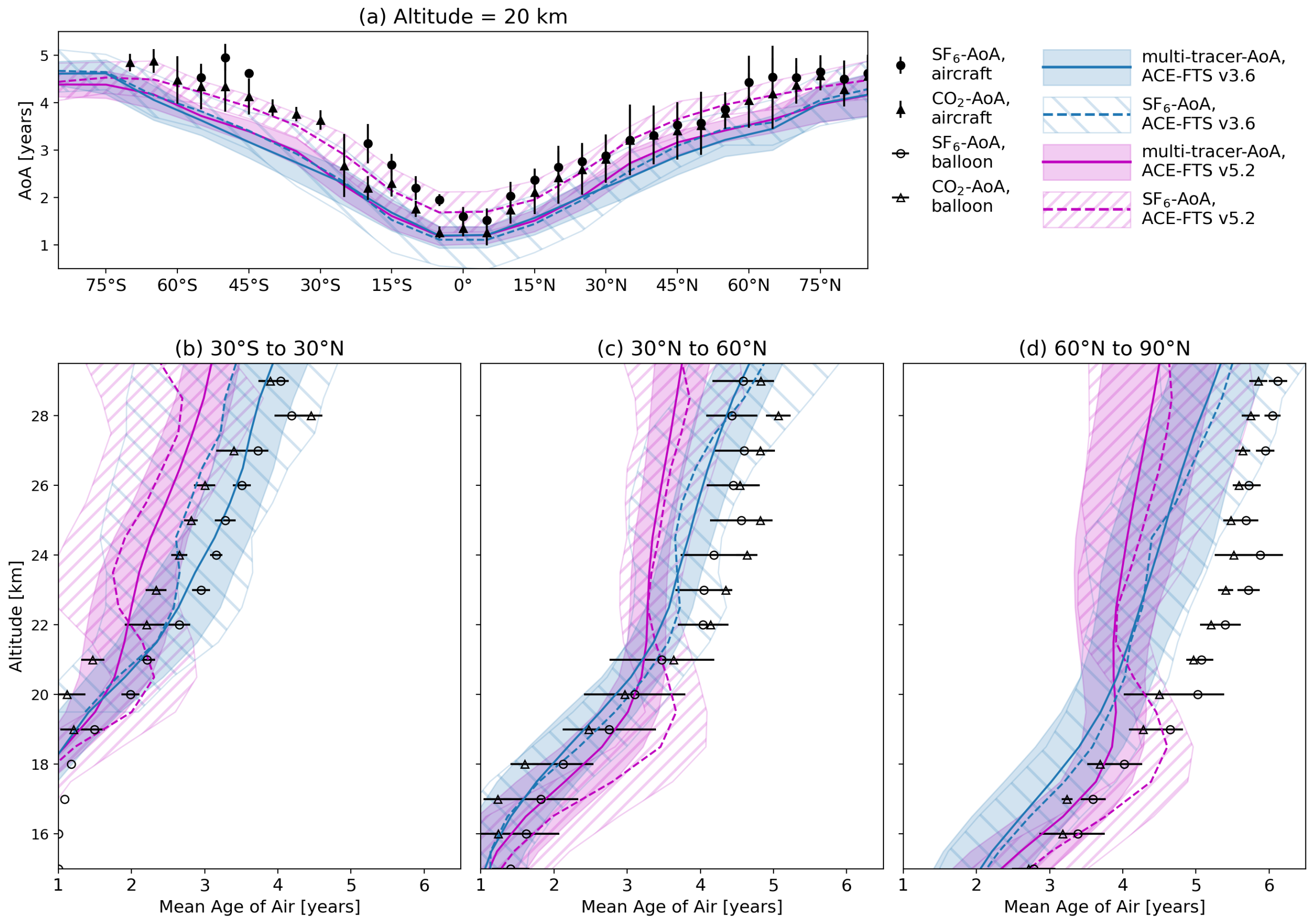

Figure 6. Comparison of estimated zonal-mean AoA profiles from the compiled dataset published by Garny et al. (2024c) with ACE-FTS profiles from dataset versions 3.6 and 5.2, sampled over the full measurement periods at corresponding latitudes and altitudes. Circles and triangles denote AoA from the compiled dataset based on in situ measurements of SF_6/CO_2 from aircraft campaigns (black fill) and balloon launches (transparent). Magenta lines, shading and diagonal hatching (left to right) show results for dataset version 5.2, and blue lines, shading and diagonal hatching (right to left) show results for dataset version 3.6. Dashed lines with diagonal hatching indicate SF_6-only AoA derived from the means and standard deviations of the sampled SF_6 profiles, while solid lines with shading indicate the sample-mean multi-tracer AoA plus/minus one standard deviation.

altitude. This feature is apparently smoothed out in the multi-tracer AoA. The second is the lower AoA estimate for dataset version 5.2 compared with version 3.6 above roughly 20 km, and vice versa below roughly 20 km, for both types of AoA estimate.

For the assessment of the AoA estimation methods and ACE-FTS datasets, we calculated the mean squared residual (MSR) for all in situ measurements and the corresponding ACE-FTS-based AoA estimates for both methods and both datasets. The

https://doi.org/10.5194/egusphere-2026-4647
Preprint. Discussion started: 2 September 2026

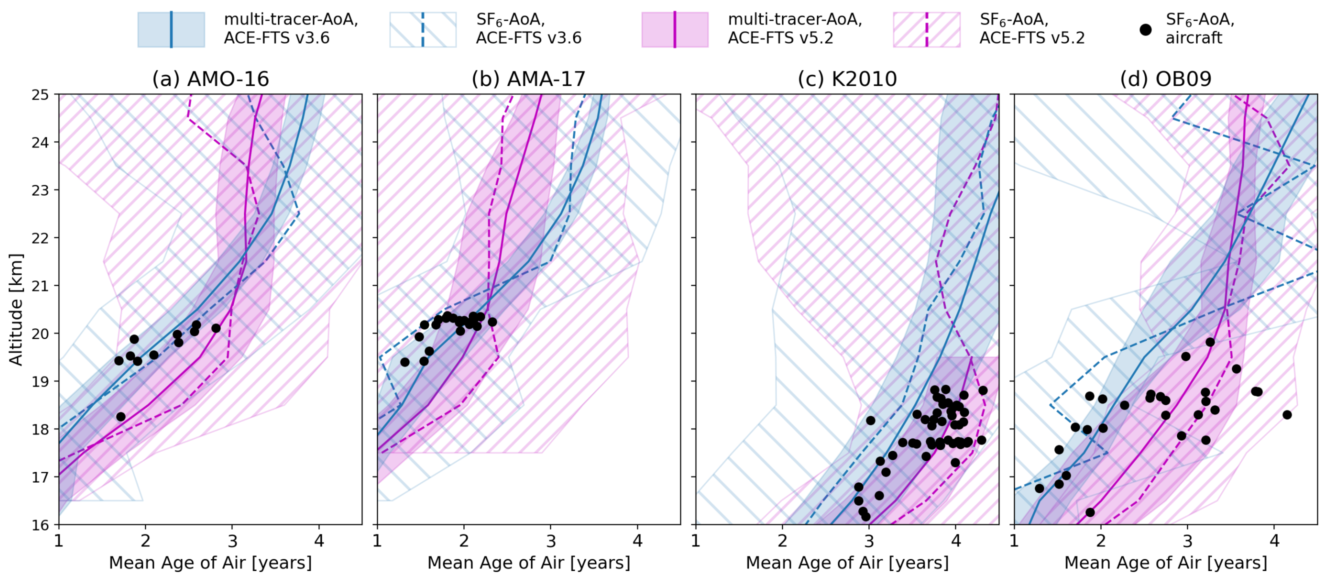

Figure 7. Comparison of AoA derived from SF_6 measurements during the Geophysica campaigns (Table 1) with ACE-FTS profiles from dataset versions 3.6 and 5.2, sampled 20 days before and after the campaign midpoints using latitudes up to 7.5° below and above the mean latitude of all flights. Black dots denote AoA from aircraft SF_6 measurements (convolution method with sink correction). Magenta lines, shading and diagonal hatching (left to right) show results for dataset version 5.2, and blue lines, shading and diagonal hatching (right to left) show results for dataset version 3.6. Dashed lines with diagonal hatching indicate SF_6-only AoA derived from the means and standard deviations of the sampled SF_6 profiles, while solid lines with shading indicate the sample-mean multi-tracer AoA plus/minus one standard deviation.

resulting MSR values are listed in Table 3. Focusing first on the AoA estimation methods, the results are rather unambiguous. For the aircraft campaigns, the AirCore flights, and the vertical profiles of the compiled dataset for the tropical and mid-latitude bands, the MSR values for the multi-tracer AoA are all lower than the corresponding values for the SF_6-only AoA, in some cases even significantly lower. The remaining two cases in the compiled dataset — vertical profiles at high latitudes and the

Table 1. Overview of M55 Geophysica high-altitude aircraft campaigns

Campaign	Date	Location	Latitude	Altitude (km)	Reference
OB09	30 Oct 2009 4 Nov 2009	Oberpfaffenhofen, Germany	48–54°N	10–20	(Leedham Elvidge et al., 2018)
K2010	20 Jan 2010 2 Feb 2010	Kiruna, Sweden	62–77°N	9–19	(Leedham Elvidge et al., 2018)
AMO-16	1 Sep 2016 6 Sep 2016	Kalamata, Greece	33–41°N	10–20	(Adcock et al., 2021)
AMA-17	27/29/31 Jul 2017 2/4/6 Aug 2017	Kathmandu, Nepal	21–29°N	10–20	(Adcock et al., 2021)

https://doi.org/10.5194/egusphere-2026-4647
Preprint. Discussion started: 2 September 2026

Table 2. AirCore launch dates in spring and fall 2018 at ∼ 52.4°N from Norwich, England (Laube et al., 2020)

1st spring flight	2nd spring flight	1st fall flight	2nd fall flight
1 May 2018	14 May 2018	26 Sep 2018	10 Oct 2018
11.5–28.9 km	12.1–28.6 km	11.7–25.7 km	12.7–26.4 km

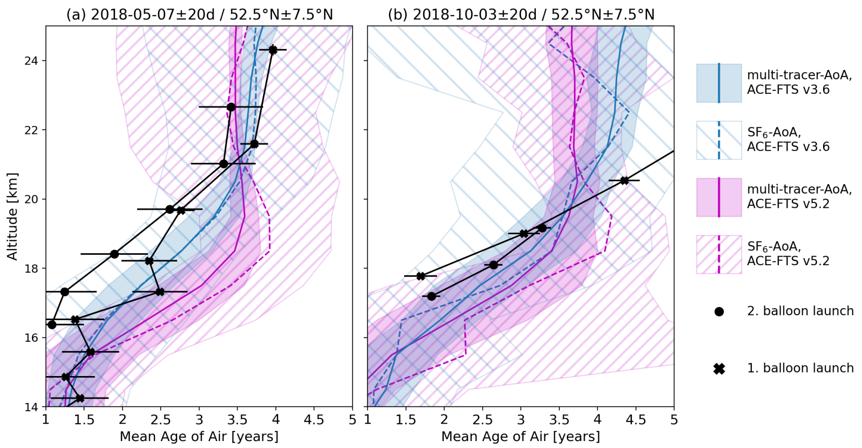

Figure 8. Comparison of AoA derived from SF_6 measurements during the AirCore flights (Table 2) with ACE-FTS profiles from dataset versions 3.6 and 5.2, sampled 20 days before and after the day between the two flights in each season, using latitudes up to 7.5° below and above the mean latitude of the two flights. Black dots denote AoA from AirCore SF_6 measurements (convolution method with sink correction). Magenta lines, shading and diagonal hatching (left to right) show results for dataset version 5.2, and blue lines, shading and diagonal hatching (right to left) show results for dataset version 3.6. Dashed lines with diagonal hatching indicate SF_6-only AoA derived from the means and standard deviations of the sampled SF_6 profiles, while solid lines with shading indicate the sample-mean multi-tracer AoA plus/minus one standard deviation.

horizontal profile at 20 km — show the opposite behavior and stand out from the other cases in several respects; they are discussed later.

For the four cases mentioned above, the better agreement of the multi-tracer AoA can largely be explained by the reduced uncertainty and smoother, less erratic profiles, especially for version 3.6, as well as by the reduction of the S-shaped curve (secondary maximum in AoA) in dataset version 5.2. The S-shaped curve in the SF_6-only AoA, caused by the secondary AoA maximum, is not observed in the AoA profiles derived from the in situ data and leads to an overestimation of AoA somewhere between 16 km and 20 km, depending on latitude. This overestimation appears to be reduced by the multi-tracer method. For the vertical profiles in the compiled dataset in the tropical latitude band (Figure 6(b)), SF_6-only AoA is noticeably younger and in poorer agreement with the in situ AoA than the multi-tracer AoA above ∼22 km for both datasets. This could indicate a bias toward too high SF_6 values in the tropics for both datasets, which is reduced by the multi-tracer method.

https://doi.org/10.5194/egusphere-2026-4647
Preprint. Discussion started: 2 September 2026

Table 3. Mean squared residual (MSR) for AoA in years^2 derived from the considered in situ measurements (aircraft campaigns: Table 1; AirCore launches: Table 2; compiled dataset: Garny et al. (2024c)) and the corresponding ACE-FTS-based AoA estimates using the SF_6-only and multi-tracer methods for dataset versions 3.6 and 5.2.

in situ measurements			**Version 3.6**		**Version 5.2**	
			SF_6-only	**multi-tracer**	**SF_6-only**	**multi-tracer**
Aircraft campaigns	OB09		1.61	0.72	0.64	0.42
	K2010		0.45	0.23	0.29	0.10
	AMO-16		0.09	0.07	0.63	0.32
	AMA-17		0.17	0.05	0.28	0.13
AirCore flights	Spring 1		0.24	0.23	0.98	0.62
	Spring 2		0.43	0.42	1.97	1.23
	Fall 1		2.46	1.58	3.10	2.37
	Fall 2		0.18	0.10	0.98	0.34
Compiled dataset Balloons	30°S – 30°N	SF_6	0.31	0.05	1.14	0.72
		CO_2	0.26	0.19	0.88	0.43
	30°N – 60°N	SF_6	0.15	0.13	0.52	0.47
		CO_2	0.34	0.30	1.12	0.94
	60°N – 90°N	SF_6	0.74	0.96	1.13	1.51
		CO_2	0.43	0.51	0.81	0.99
Compiled dataset Aircrafts	20 km	SF_6	0.63	0.72	0.13	0.59
		CO_2	0.31	0.41	0.05	0.29

Having shown that the multi-tracer AoA is generally in better agreement with the in situ AoA, we now compare the two dataset versions against the in situ measurements in more detail. Considering all vertical profiles, including the previously excluded high-latitude profiles of the compiled dataset, but still excluding the 20 km horizontal profile for now, the MSR values in Table 3 are lower for dataset version 3.6 than for dataset version 5.2 in all cases except the two aircraft campaigns OB09 and K2010. For campaign OB09, however, the spread of the in situ AoA values is significantly higher than for the other campaigns, making interpretation difficult. Campaign K2010 is the only one of the four campaigns conducted in the high-latitude region between 60°N and 90°N. The results for the previously excluded high-latitude profiles of the compiled dataset in Figure 6(d) suggest that, at the flight altitudes of campaign K2010, from roughly 16 km to 19 km, AoA estimates from dataset version 5.2 are indeed in better agreement with the in situ AoA than AoA estimates from dataset version 3.6, at least for the multi-tracer AoA. This better agreement of version 5.2 in this particular altitude and latitude range, however, seems to be caused by the S-shaped curves of the profiles, which can otherwise lead to an overestimation of AoA in the considered altitude range in the lower latitude bands. Considering the entire altitude range, even the profiles for version 3.6 are too low compared to the in situ AoA profiles, which is not the case for the other latitude bands, or at least not to the same extent. This apparent bias toward too low AoA values could be caused by a bias toward too high SF_6 values in the high-latitude region,

https://doi.org/10.5194/egusphere-2026-4647
Preprint. Discussion started: 2 September 2026

as it is also present in the SF_6-only AoA of version 3.6. Another explanation could be the small number of balloon-launches used to compile the in situ AoA profiles, as suggested by Garny et al. (2024b). Perhaps particularly old air masses from the polar vortex region were sampled by these balloon, making the final compiled result not representative for the entire region. For a fair comparison between the two AoA estimation methods in the high-latitude region, this bias would have to be further investigated and corrected if need be. This, however, would require more in situ measurements at all considered altitudes and latitudes, which are unfortunately not available at the moment.

The horizontal profile at 20 km in the compiled in situ dataset does not appear to be consistent with the other in situ measurements. With the exception of the SF_6-only AoA for dataset version 5.2, it lies above all ACE-FTS-based AoA profiles at almost every latitude. By contrast, it agrees well with the SF_6-only AoA for dataset version 5.2 at almost every latitude. However, the other in situ AoA profiles suggest that the SF_6-only AoA of dataset version 5.2 is too high at lower and midlatitudes and may agree well with the in situ AoA only in the high-latitude region. Note that aircraft campaigns OB09 and K2010, as well as the second balloon flight in fall 2018, cannot be used to support this conclusion because data above 20 km are lacking. The results for the first AirCore flight in fall 2018 (Figure 8) agree better with the SF_6-only AoA of dataset version 5.2 at 20 km than with the other ACE-FTS-based AoA estimates, but this flight appears to be an outlier because its AoA-altitude gradient is much steeper than that of the other AirCore data. There may therefore be an issue with some of the aircraft measurements included in the compiled horizontal profile at 20 km, which could explain the discrepancy with the other in situ measurements. For example, SF_6 calibration issues were reported for the SOLVE mission (Ray et al., 2024), and data from that mission are included in the compiled horizontal profile.

Overall, dataset version 3.6 shows better agreement with the in situ measurements than version 5.2. The S-shaped structure present in the SF_6-only AoA profiles of version 5.2—only partially reduced in the multi-tracer AoA—is not observed in the in situ data and is therefore likely caused by an artefact in the SF_6 retrieval. Such a feature is also absent in SF_6-derived AoA products based on MIPAS satellite measurements, which further supports this interpretation (e.g. Stiller et al., 2008; Haenel et al., 2015).

Below about 20 km, application of the multi-tracer method in version 5.2 reduces this artefact and leads to improved agreement with the in situ profiles. This is particularly evident in comparisons with the compiled dataset, where the multi-tracer AoA for version 5.2 agrees comparably well with the in situ AoA as version 3.6 up to $\sim$20 km. More generally, the ACE-FTS multi-tracer AoA shows better agreement with the in situ reference data than the SF_6-only product.

3.4 Trend analysis

Ploeger et al. (2021) showed that trend estimates can remain strongly affected by decadal variability even over 30-year periods. Given the limited temporal coverage of the ACE-FTS record, which spans roughly 20 years, robust detection of an underlying long-term trend is therefore challenging. Recent studies by Dubé et al. (2025) and Saunders et al. (2025) investigated AoA trends derived from ACE-FTS data using different methods and reached differing conclusions. Here, we analyze trends over the period 2004–2021 using the new multi-tracer AoA product based on ACE-FTS measurements. Because this product is derived

https://doi.org/10.5194/egusphere-2026-4647
Preprint. Discussion started: 2 September 2026

using a different methodology and is largely independent of a priori model data (see Sect. 2.3), it provides an informative basis for comparison with previously published results.

Smoothed time series with uncertainty envelopes were created for the monthly zonal-mean time series (see end of Sect. 2.3) of the multi-tracer AoA of both datasets and the CLaMS clock tracer AoA using Gaussian process regression (see the
500 lookup-table construction in Sect. 2.3). Following Ray et al. (2020), a 5 year window was chosen for smoothing to suppress measurement noise and short-period variability such as seasonality and the quasi-biennial oscillation (QBO). Signals with longer, less predictable periods, such as the El Niño–Southern Oscillation (ENSO), cannot be averaged out as effectively given the limited record length.

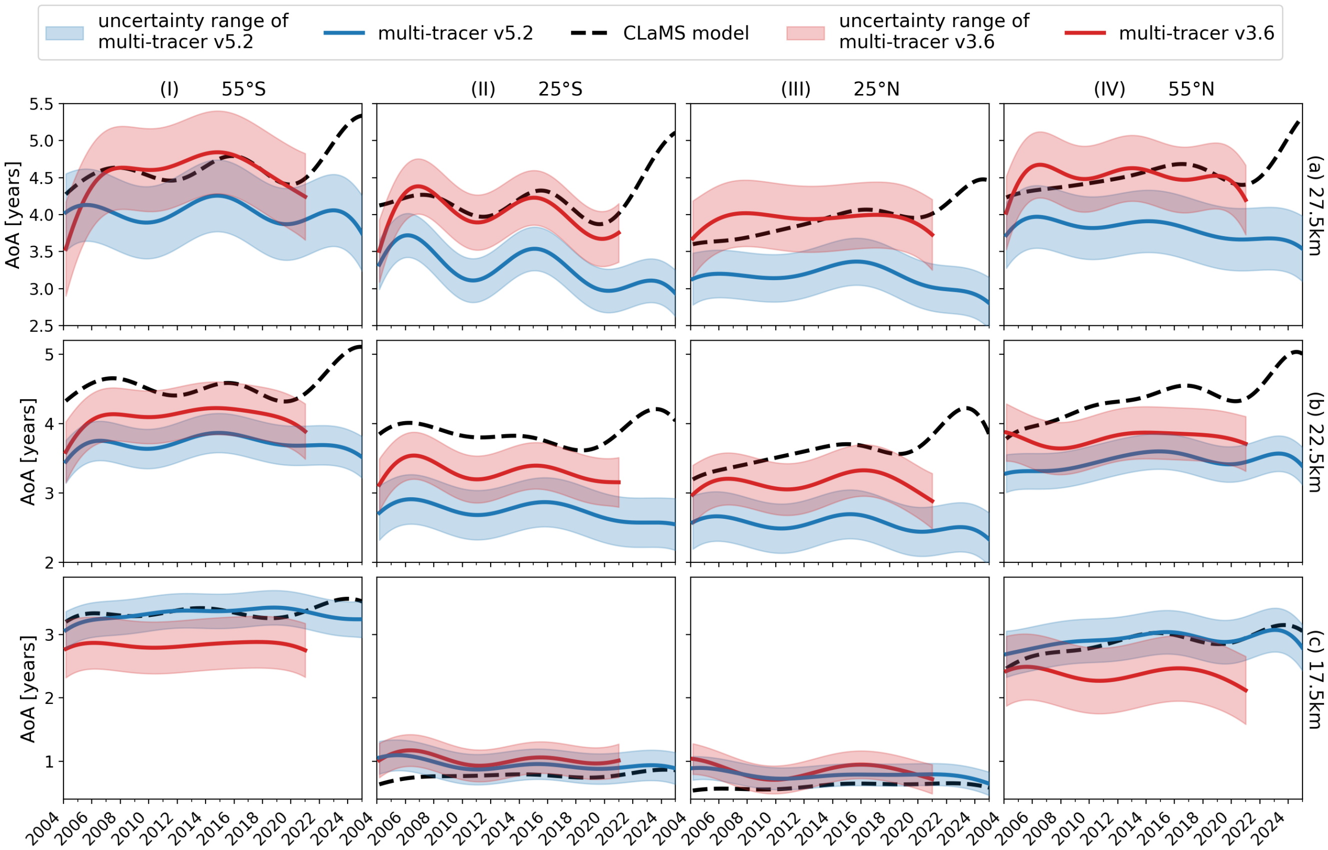

Figure 9. Smoothed monthly zonal-mean time series of multi-tracer AoA for ACE-FTS dataset version 3.6 (solid red line with red uncertainty shading), ACE-FTS dataset version 5.2 (solid blue line with blue uncertainty shading), and CLaMS clock tracer AoA (dashed black line). Columns (I)–(IV) show the same 10° latitude bands (bin means indicated above), and rows (a)–(c) show the same altitude levels (indicated on the right-hand side).

Figure 9 illustrates the smoothed time series at three representative altitude levels and four latitude bands. As noted in
505 Sect. 3.2, AoA in version 5.2 is lower than in version 3.6 above roughly 20 km, whereas at the lowest altitude level version 5.2

https://doi.org/10.5194/egusphere-2026-4647
Preprint. Discussion started: 2 September 2026

yields comparable values at 25°S and 25°N and higher values at 55°S and 55°N. This discrepancy likely reflects differences in the retrieval algorithms between the two versions. Despite this, the AoA time series in the two datasets generally follow similar trajectories. The version 3.6 results are more erratic at the beginning of the observation period (row (a), columns (I), (II), and (IV)), and their uncertainty envelopes are larger in most regions shown, likely because of the greater sparsity compared with version 5.2. Note that the lower sparsity in version 5.2 is the result of the updated retrieval algorithm, which allows for fewer discarded occultations.

Long-period oscillations are clearly visible in the smoothed time series for all three AoA estimates, including the CLaMS clock tracer AoA (especially in the southern hemisphere). These decadal variations are likely a result of superposition of different variability factors. Strahan et al. (2020) have proposed that the combination of the QBO with the seasonal cycle could have the potential to cause similar low-frequency variability. Differences between the ACE satellite and CLaMS model AoA become especially evident in the pronounced increase in the smoothed CLaMS clock tracer AoA around 2021 at almost every latitude and altitude. No comparable increase around that time is observed in the corresponding AoA time series of dataset version 5.2. It should be noted that the measurement period for dataset version 3.6 ends in early 2021, which limits a direct comparison of this feature between the two datasets. The extent to which the pronounced increase in the CLaMS clock tracer AoA at the end of the record is related to natural variability, such as the QBO or the 2022 Hunga Tonga–Hunga Ha'apai eruption, remains an open question and warrants further investigation.

We analysed correlations and trends of the (unsmoothed) monthly zonal-mean multi-tracer AoA, SF_6-only AoA and CLaMS clock tracer AoA for both datasets. These correlations and trends reflect the behaviour of the respective AoA estimates over the limited measurement periods and could be influenced by low-frequency oscillations in the timeseries, as determination of forced long-term trends in stratospheric AoA generally requires observational records of ≤ 30 years (Ploeger et al., 2021). The respective correlation coefficient is

$$\rho = \frac{\mathrm{cov}\,(\mathrm{AoA}, t)}{\sigma_{\mathrm{AoA}}, \sigma_t}. \qquad (5)$$

Here t denotes time, σ_{AoA} and σ_t are the standard deviations of AoA and t, respectively, and $\mathrm{cov}(\mathrm{AoA}, t)$ is their covariance. Linear trends over the respective measurement periods were then obtained from the correlation coefficients via

$$m = \rho \frac{\sigma_{\mathrm{AoA}}}{\sigma_t}, \qquad (6)$$

where m represents the slope of the linear regression of AoA with respect to time.

We computed two-tailed p-values for each correlation, under the null hypothesis of no correlation, using `scipy.stats.pearsonr`. The linear trends over the period 2004 to 2021, which is the full period covered by dataset version 3.6, for the multi-tracer AoA of both datasets and the CLaMS clock tracer AoA are shown in Figure 10; Figure D3 in the Appendix shows the corresponding results for the SF_6-only AoA of both datasets over the same period. Locations with p-values below 5% are marked with an “X” in both figures. A p-value below 5% indicates that, under the null hypothesis, the probability of observing

https://doi.org/10.5194/egusphere-2026-4647
Preprint. Discussion started: 2 September 2026

a correlation at least as extreme as the measured one is less than 5%; such correlations are therefore unlikely to arise from random sampling alone, although effect size and physical plausibility must still be considered. All correlations and trends discussed in the following are derived from the original (unsmoothed) time series rather than from the smoothed data shown in Fig. 9, as the smoothing is intended solely for visualization. While the resulting trends are similar, smoothing substantially increases the correlation coefficients and leads to uniformly very low p-values across most regions, reducing the discriminative power of the statistical significance test.

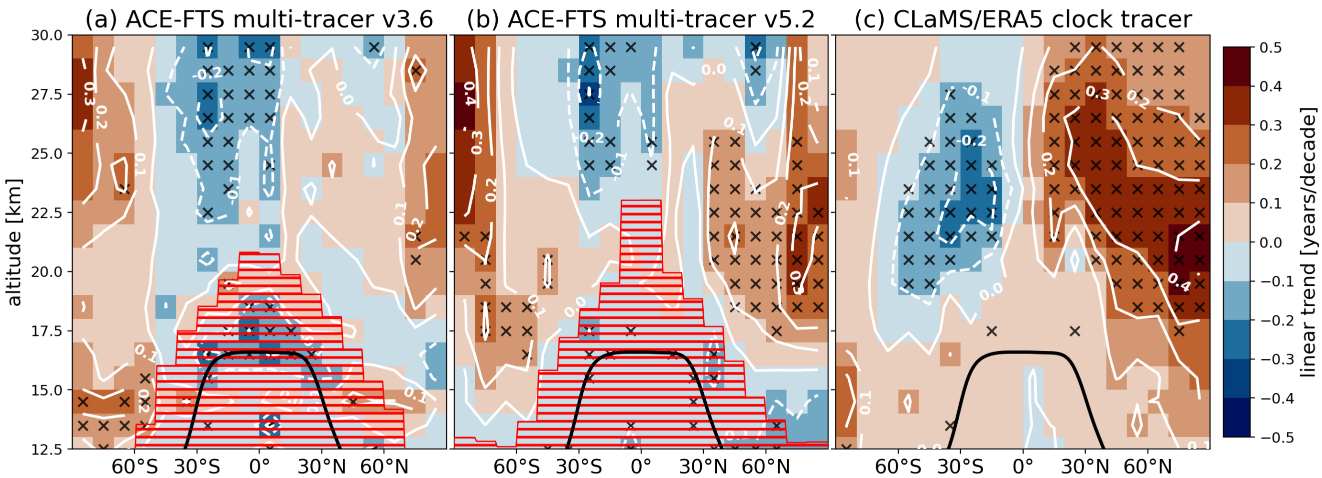

Figure 10. Linear trends according to Eq. 6 for three unsmoothed monthly zonal-mean AoA estimates based on ACE-FTS observations and CLaMS model results over the period 2004 to 2021: multi-tracer AoA for ACE-FTS v3.6 (a), multi-tracer AoA for ACE-FTS v5.2 (b), and CLaMS clock tracer AoA (c). Thick black lines indicate the mean tropopause height over the full measurement period, derived from ERA5 reanalysis. Locations marked with an "X" denote p-values below 0.05. Red horizontal hatching indicates regions where AoA estimates fall below the threshold of 1.5 years.

The linear trends in Figure 10 for the multi-tracer AoA of both datasets show the same broad features and are generally in good agreement. In the Northern Hemisphere extratropical stratosphere, AoA increases between approximately 15 and 28 km. In contrast, AoA decreases in the tropics and southern subtropics above roughly 20 km. Together, these features form a pronounced hemispheric dipole pattern. This pattern is opposite to the expectation from ozone recovery, which would suggest a weakening of this asymmetry (cf. Ploeger and Garny, 2022). The spatial structure and sign of the trends are in qualitative agreement with the CLaMS AoA based on ERA5. These results are consistent with Dubé et al. (2025), who reported increasing AoA trends in the Northern Hemisphere between 100 hPa (∼16 km) and about 10 hPa (∼30 km), decreasing trends above, and a negative AoA trend in the Southern Hemisphere subtropics around 20 hPa (∼27 km). The linear trends for the SF_6-only AoA for both datasets (Appendix, Figure D3) exhibit substantial noise and agree rather poorly with the corresponding values for the multi-tracer AoA.

Saunders et al. (2025) found slight negative AoA trends between 14 km and 20 km and 40°to 70°latitude in both hemispheres. The trends of the four ACE-FTS-based AoA estimates in this study do not agree well in the narrower region investi-

https://doi.org/10.5194/egusphere-2026-4647
Preprint. Discussion started: 2 September 2026

gated by Saunders et al. (2025). Similar negative AoA trends to those reported by Saunders et al. (2025) appear in the SF_6-only AoA results for version 5.2 (Appendix, Figure D3 (b)) up to roughly 16 km across all latitudes, and in the multi-tracer AoA results for version 3.6 in the Northern Hemisphere around 60°latitude and 17 km altitude. Overall, the AoA trends from the multi-tracer method applied to ACE data corroborate published results that the Northern hemispheric circulation has slowed down over the last 2-3 decades (cf. Stiller et al., 2017; Mahieu et al., 2014; Ploeger et al., 2021). The ultimate cause for this variability is still a matter of debate.

For both dataset versions 5.2 and 3.6 (Appendix, Figure D3), linear trends for SF_6-only AoA exhibit substantially noisier and less coherent patterns than those for the multi-tracer AoA. The correlations and linear trends in version 3.6 resemble those of version 5.2, but regions of negative correlation — particularly near the tropopause — are markedly smaller in extent. Regarding the results for the multi-tracer AoA, version 5.2 depicts significantly stronger correlations and more p-values below 5% in the northern hemisphere. Differences between the two datasets can be attributed to the sparser sampling and to the updated retrieval algorithm implemented in version 5.2.

Overall, the trend analysis reveals a consistent large-scale pattern across both ACE-FTS versions, characterized by increasing AoA in the Northern Hemisphere extratropical stratosphere and decreasing AoA in the tropics and subtropics above $\sim$ 20 km in the Southern Hemisphere, forming a robust hemispheric dipole. This pattern is evident in both datasets, although the signals are generally weaker and less spatially coherent in version 3.6, likely due to its sparser sampling. The sign of the trends in both hemispheres is in qualitative agreement with the ERA5-based CLaMS clock tracer AoA, while the magnitude of the changes is smaller in the observational estimates. Taken together, these results are consistent with previous studies and support the picture of a recent slowdown in Northern Hemisphere circulation, albeit with substantial uncertainty in the underlying drivers.

4 Summary and Conclusions

Building on our previous work (Voet et al., 2025), we further developed the multi-tracer method for deriving stratospheric mean age of air (AoA) and applied it to ACE-FTS observations from the Canadian SCISAT satellite. We applied the method to ACE-FTS dataset versions 3.6 and 5.2, and for comparison we also applied a conventional SF_6-only approach based on the convolution method with sink correction to both datasets. To demonstrate the advantages of the multi-tracer method in terms of accuracy and precision, we recreated the two ACE-FTS datasets in the CLaMS model using the six required trace gases SF_6, N_2O, CFC-11 (CCl_3F), CFC-12 (CCl_2F_2), HCFC-22 ($CHClF_2$), and CH_4. In the model, the true AoA can be calculated precisely from an implemented ideal clock tracer. We then derived AoA for the recreated datasets with both methods and compared the results with the true model AoA as a proof of concept. Independent of the dataset, the results indicate that the uncertainty of zonal-mean AoA can be reduced by about 50% with the multi-tracer method, while AoA at individual observation points can be estimated with an average uncertainty of approximately 0.3 years. This suggests that the multi-tracer method is suitable for interpreting spatially resolved AoA, unlike SF_6-only AoA from satellite data, which generally requires zonal averaging because of the large measurement uncertainty.

https://doi.org/10.5194/egusphere-2026-4647
Preprint. Discussion started: 2 September 2026

Consistent with the proof-of-concept results, the multi-tracer method substantially reduced noise in the AoA derived from the actual ACE-FTS datasets 3.6 and 5.2, as shown by the zonal means for two representative three-month periods in Figure 5 for version 5.2 and Figure D1 for version 3.6. For version 3.6, the noise reduction is also visible, though more subtly, in the zonal-mean values over the full observation period in Figure 3. The figure also reveals a layer of decreasing AoA with increasing altitude in the SF_6-only AoA for version 5.2 (panel d), which is not present in the other three AoA estimates. The comparison with in situ AoA estimates from SF_6 and CO_2 (Figures 7 to 6) suggests that this S-shape in the SF_6-only AoA altitude profile is likely an artefact of the updated SF_6 retrieval algorithm used in dataset version 5.2. The in situ AoA profiles appear to agree more closely with version 3.6 than with version 5.2, and with the multi-tracer AoA than with the SF_6-only AoA. The aircraft measurements in the compiled dataset (Figure 6a) suggest a different picture and conflict with the remaining in situ measurements. Resolving this conflict would require further investigation, which is beyond the scope of this study. The in situ AoA profiles in the compiled dataset for the high-latitude band (60°N–90°N) agree poorly with all four ACE-FTS-based AoA estimates. Garny et al. (2024b) noted a similar poor agreement between satellite measurements and the compiled dataset in the high-latitude band and suggested that the compiled dataset may not be representative of the entire high-latitude band because the number of measurements may be too small. Another possible explanation is inconsistent sampling, for both the in situ and satellite observations, near the edges of the polar vortex, where variability is very high. A definitive conclusion about possible systematic errors in the ACE-FTS datasets would require a better criterion for defining the vortex edges, as well as many more in situ measurements across the full altitude and latitude range; such data are not currently available.

The smoothed monthly zonal-mean time series of the multi-tracer AoA for both datasets show low-frequency oscillations with an approximate decadal period and underlying trends (Fig. 9). The linear trends in the latitude–altitude plane exhibit smoother and more coherent patterns for the multi-tracer AoA compared to the standard SF_6-based AoA in both datasets (Figs. 10 and D3). At least in the northern hemisphere, trends are stronger and p-values below 5% more frequent for the multi-tracer AoA of dataset version 5.2 than for the more sparse dataset version 3.6. The multi-tracer method therefore appears better suited for long-term trend analysis, although longer records are required to determine the long-term trends in AoA more definitively. The linear trends emerging from the ACE-based multi-tracer AoA data show a clear increase in AoA in the Northern hemisphere over the period 2004-2021, indicating a slow-down of the stratospheric circulation in this hemisphere. In the tropics and Southern hemisphere subtropics, AoA decreases over this period. This hemispheric dipole pattern in AoA trends over the last 2-3 decades is largely consistent with other recent studies (cf. Dubé et al., 2025; Ploeger and Garny, 2022) and indicates a circulation slow-down in the NH relative to the SH. The ultimate causes for these changes are still unclear an warrant further investigation.

https://doi.org/10.5194/egusphere-2026-4647
Preprint. Discussion started: 2 September 2026

Appendix A: Accounting for biases in SF_6 and AoA

A1 Accounting for biases in SF_6 mixing ratios of ACE-FTS dataset version 3.6 and 5.2

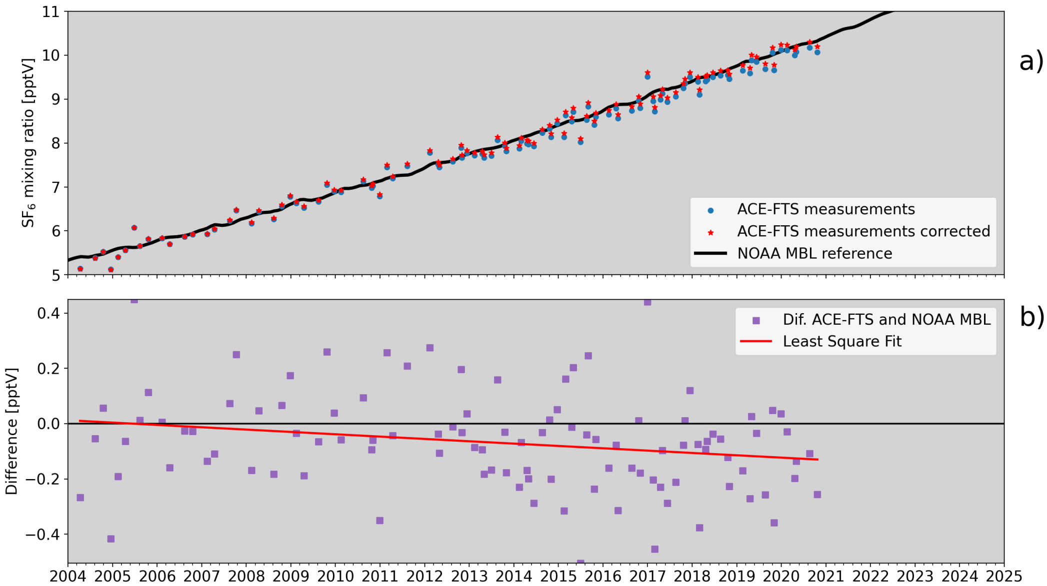

Figure A1. a): Thick black line: SF_6 reference time series $SF_{6,\mathrm{ref}}(t)$ (mostly based on NOAA MBL, see Garny et al. (2024b)). Blue dots: Monthly and zonally averaged tropical tropospheric SF_6 mixing ratios in ACE-FTS dataset version 3.6. Red stars: Corrected SF_6 reference time series to account for measurement bias. b): Blue dots: Difference between ACE-FTS measurements and uncorrected SF_6 reference time series (Blue dots minus black line in panel a)). Red line: Least square fit of polynomial with smallest BIC and AIC

Table A1. Bayesian Information Criterion (BIC) and Akaike information criterion (AIC) for least square fits of polynomials to the differences between reference SF_6 and SF_6 in ACE-FTS dataset version 3.6

	order 0	order 1	order 2	order 3
AIC	-363	-366	-366	-366
BIC	-363	-364	-361	-359

The creation of the corrected reference time series is illustrated in Figure A1. First, a time series of monthly zonal-mean SF_6 mixing ratios at tropical latitudes and tropospheric altitudes (using the same definitions for both regions as in Saunders et al. (2025)) was constructed from dataset version 3.6 (blue dots in panel a). The tropopause height at each point and time of observation was interpolated from ERA5 reanalysis data. The SF_6 reference time series — entirely based on NOAA Marine Boundary Layer (MBL) data for the ACE-FTS measurement period (blue dots in panel a) — was then subtracted from the measurement-based tropical tropospheric time series (purple dots in panel b). Note that, because different datasets were used

https://doi.org/10.5194/egusphere-2026-4647
Preprint. Discussion started: 2 September 2026

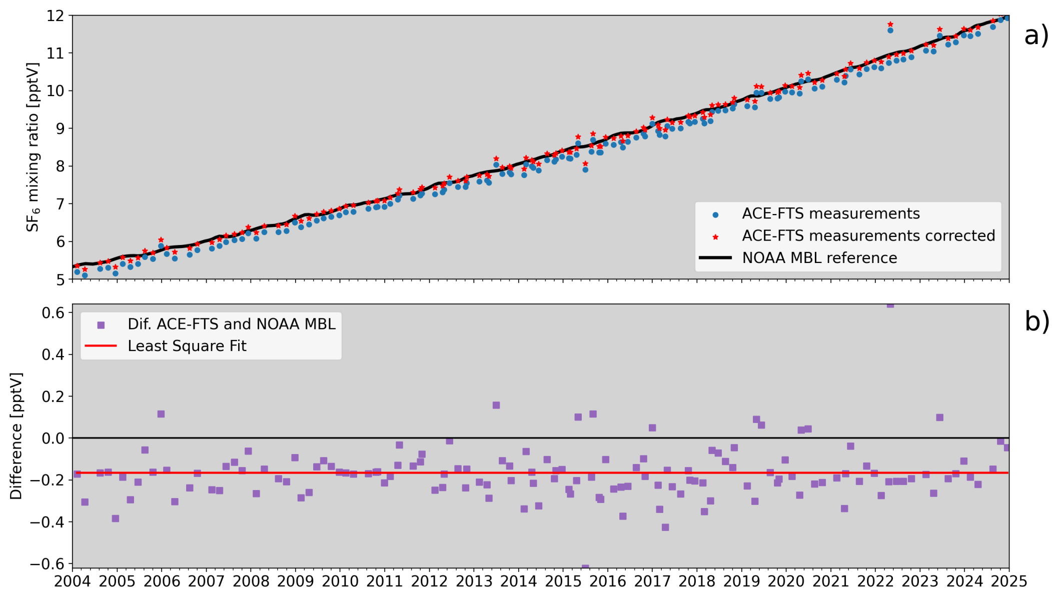

Figure A2. a): Thick black line: SF_6 reference time series $SF_{6,\mathrm{ref}}(t)$ (mostly based on NOAA MBL, see Garny et al. (2024b)). Blue dots: Monthly and zonally averaged tropical tropospheric SF_6 mixing ratios in ACE-FTS dataset version 3.6. Red stars: Corrected SF_6 reference time series to account for measurement bias. b): Blue dots: Difference between ACE-FTS measurements and uncorrected SF_6 reference time series (Blue dots minus black line in panel a)). Red line: Least square fit of polynomial with smallest BIC and AIC

Table A2. Bayesian Information Criterion (BIC) and Akaike information criterion (AIC) for least square fits of polynomials to the differences between reference SF_6 (tropical NOAA Marine Boundary Layer) and SF_6 in ACE-FTS dataset version 5.2

	order 0	order 1	order 2	order 3
AIC	-655	-653	-652	-651
BIC	-655	-651	-647	-642

for the tropopause height, the tropical tropospheric SF_6 mixing ratios derived from dataset version 3.6 are not identical to those derived by Saunders et al. (2025); however, the behaviour of this ACE-FTS-based tropical tropospheric time series relative to the NOAA MBL reference time series is qualitatively the same as in Saunders et al. (2025).

Polynomial functions up to third order were fitted to the differences between the two time series using a least-squares approach (motivated by Saunders et al., 2025). The fits were evaluated using the Akaike Information Criterion (AIC),

$$AIC = n \ln\left(\frac{RSS}{n}\right) + k \ln(n), \tag{A1}$$

and the Bayesian Information Criterion (BIC),

https://doi.org/10.5194/egusphere-2026-4647
Preprint. Discussion started: 2 September 2026

$$BIC = n \ln\left(\frac{RSS}{n}\right) + k \ln(n), \tag{A2}$$

where n is the number of data points, RSS is the residual sum of squares, and k is the number of fit parameters. The AIC and BIC provide measures of model quality by penalizing unnecessary complexity (i.e., a large number of parameters) and thus help to avoid over-fitting (Zhang et al., 2023). The lower the value of AIC/BIC, the better the agreement between fit and data. While both criteria balance goodness of fit and model complexity, the BIC generally imposes a stronger penalty on additional parameters than the AIC, particularly for large sample sizes. The resulting AIC/BIC values for the different polynomial orders are listed in table A1.

As the BIC favors a first-order polynomial and the AIC is ambiguous for polynomial orders between one and three, the first-order polynomial fit was selected as the optimal model to represent the observed behavior (red line in panel b). For each observation time t_{obs}, a correction factor

$$A_{\text{corr}}(t_{\text{obs}}) = \frac{\text{SF}_{6,\text{ref}}(t_{\text{obs}}) + \text{polynomial fit}(t_{\text{obs}})}{\text{SF}_{6,\text{ref}}(t_{\text{obs}})} \tag{A3}$$

was calculated for the ACE-FTS measurements. Although the correction factors were derived using only tropical tropospheric mixing ratios, they were applied to all ACE-FTS measurements at the corresponding observation time, regardless of latitude and altitude, following the procedure of Saunders et al. (2025). This approach assumes that the observed drift in the ACE-FTS measurements is caused by an instrumental bias independent of location. A similar correction was applied to dataset version 5.2, as illustrated in Figure A2. The resulting AIC and BIC values for the different polynomial orders are listed in Table A2. As both the AIC and BIC are lowest for a zeroth-order polynomial, the zeroth-order polynomial fit (regression line with slope = 0) was selected as the optimal model to represent the observed behavior and was used to calculate the correction factors.

Appendix B: Accounting for biases in AoA derived from convolution and multi-tracer method

The convolution method does not return an AoA value if the observed SF_6 mixing ratio exceeds the value of the reference time series at the time of observation, as this would imply a negative, and thus physically meaningless, AoA. Because the retrieved SF_6 mixing ratios have relatively large uncertainties, such exceedances occur occasionally in both ACE-FTS datasets. If the convolution method is applied to a sample in which some SF_6 values exceed the reference time series, the resulting sample-mean AoA is biased high, since the missing would-be negative values skew the result toward older ages. To avoid this bias, we first calculate the average SF_6 mixing ratio of the sample and then apply the convolution method, followed by the sink correction, to that average whenever averaged AoA values are compared.

Since the convolution method yields missing values when SF_6 mixing ratios exceed those in the reference time series at the time of observation, the lookup tables required for the multi-tracer method, as obtained directly from Gaussian process

https://doi.org/10.5194/egusphere-2026-4647
Preprint. Discussion started: 2 September 2026

regression (GPR), are biased toward higher AoA values at the upper end of the mixing ratio range. To mitigate this bias, we apply the following correction to each lookup table for every trace gas. The tracer mixing ratio value at AoA = 0 is set equal to the tropical tropospheric tracer mixing ratio on the day of the measurement, and a second-order polynomial is used in place of the GPR result for low AoA values so that the lookup table is continuously differentiable and has zero slope at AoA = 0. For the remaining mixing ratio range not covered by the polynomial, AoA is set to zero in the lookup table, thereby ensuring complete coverage. The uncertainty σ for the AoA range covered by the second-order polynomial and above is set to the constant value at the point where the polynomial connects to the GPR-based lookup table. For ACE-FTS dataset version 5.2, lookup tables for the five trace gases are illustrated for a representative single day and one latitude band in Figure C1 for the actual measurements and in Figure C2 for the CLaMS-simulated measurements. The uncorrected LUT versions are shown as dashed black lines.

Appendix C: Example lookup-table illustrations

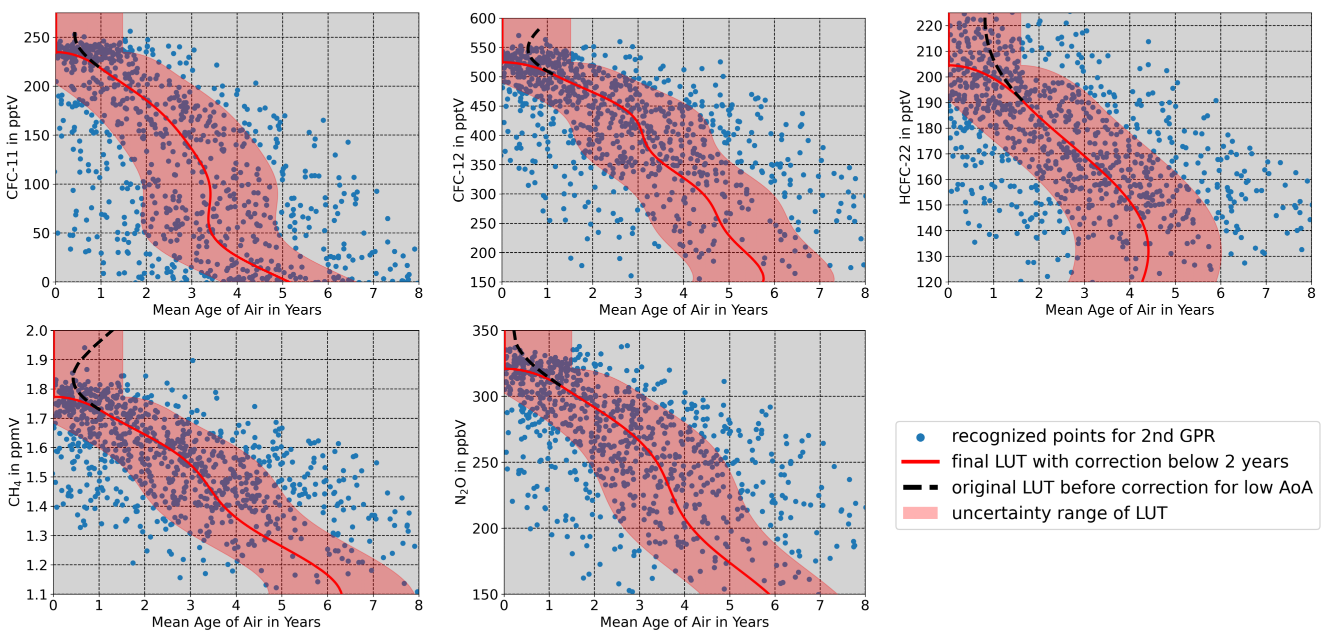

Figure C1. Lookup table (LUT) for CFC-12 in the 30°N–60°N equivalent latitude band on 11 November 2011. Blue dots: scatter plot of CFC-12 mixing ratios vs SF_6-derived AoA (convolution method) between 30°N–60°N equivalent latitude (ERA5), and between 28 November 2011 and 25 November 2011 (11 November 2011 ± 14 days) based on ACE-FTS versions 5.2. Red line and shading: AoA and ΔAoA of final LUT after second iteration and bias correction. Dashed black line: AoA of original LUT after second iteration for AoA < 2 years before bias correction. (see Text for details)

https://doi.org/10.5194/egusphere-2026-4647
Preprint. Discussion started: 2 September 2026

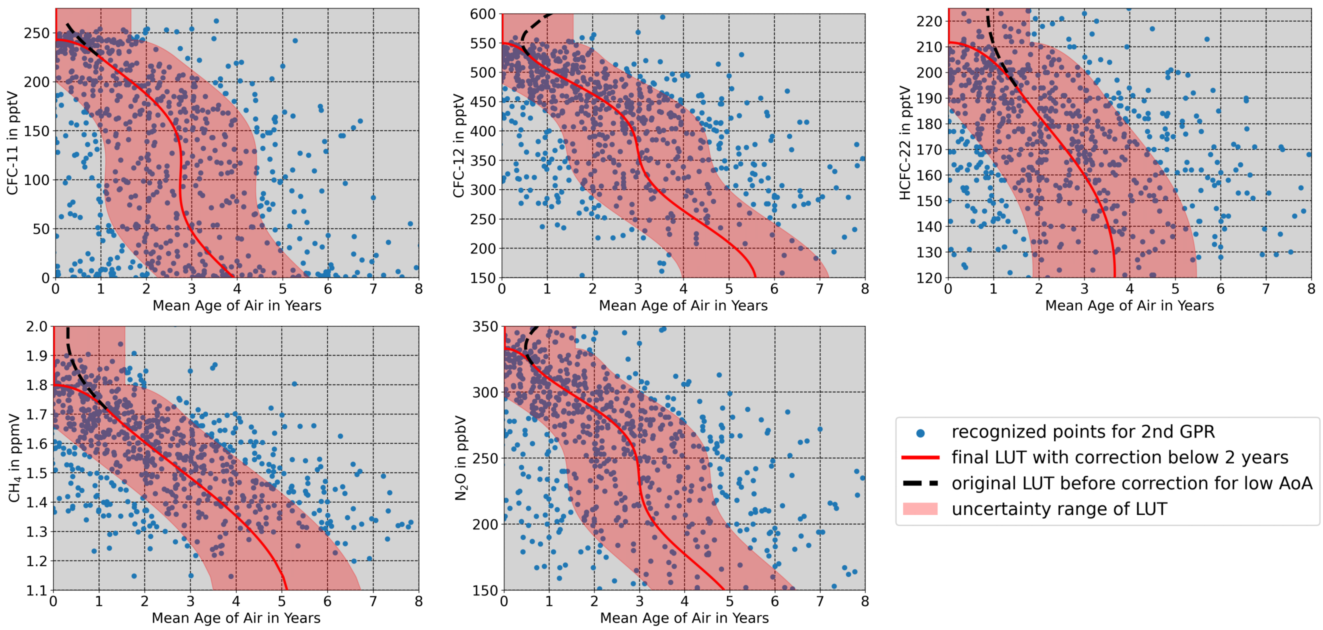

Figure C2. Same as Fig. C1, but for the CLaMS model-based synthetic measurements of ACE-FTS versions 5.2.

https://doi.org/10.5194/egusphere-2026-4647
Preprint. Discussion started: 2 September 2026

670 **Appendix D: Other Figures**

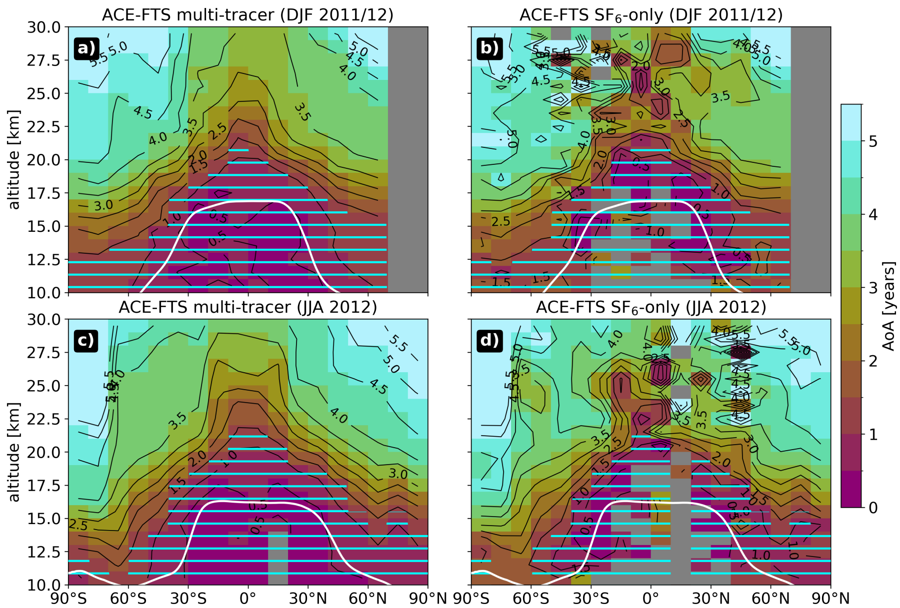

Figure D1. Same as Fig. 5, but for ACE-FTS dataset version 3.6

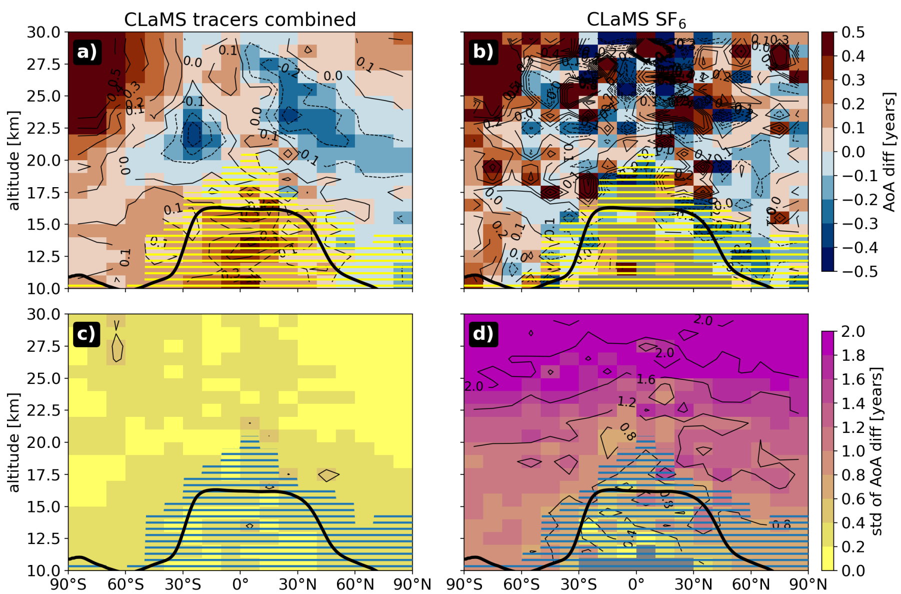

Figure D2. Same as Fig. 2, but for the period June–August 2012.

https://doi.org/10.5194/egusphere-2026-4647
Preprint. Discussion started: 2 September 2026

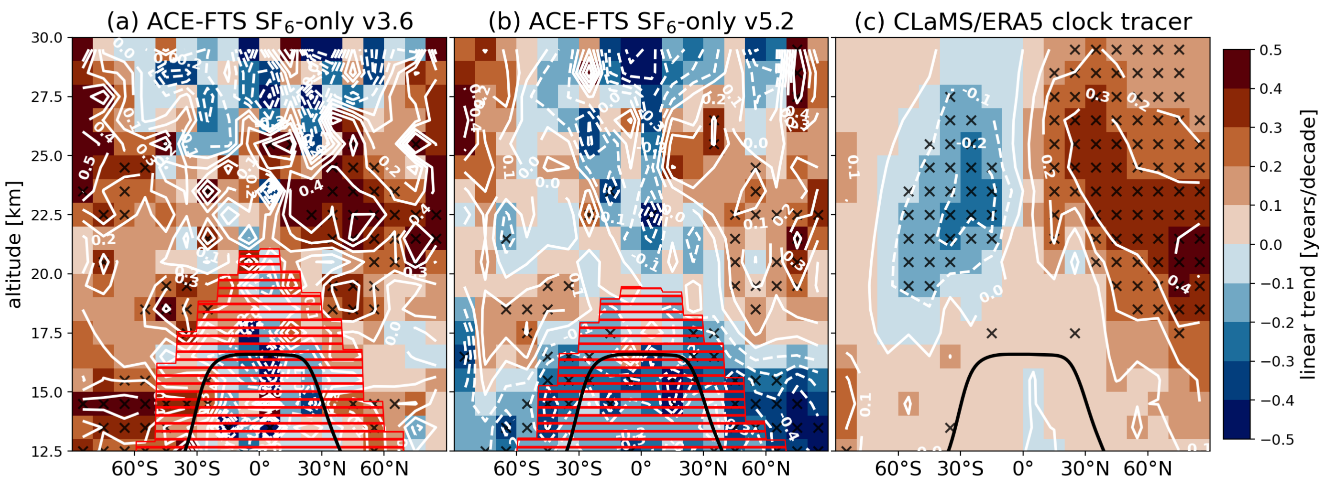

Figure D3. Same as Fig. 10, but for SF_6-only AoA

https://doi.org/10.5194/egusphere-2026-4647
Preprint. Discussion started: 2 September 2026

Code and data availability. The ACE-FTS Level 2 data used in this study can be obtained via the ACE-FTS website https://databace.scisat.ca/level2/ (registration required). The CLaMS model is available in the Modular Earth Submodel System (MESSy) Git repository at https://gitlab.dkrz.de/users/sign_in (MESSy Consortium, 2026; login required). Detailed information is available at https://messy-interface.org/licence/application (last access: 14 July 2026). The implementation of the CLaMS model in the MESSy framework is described by Hoppe et al. (2014). ERA5 reanalysis data are available from the European Centre for Medium-Range Weather Forecasts (Hersbach et al., 2023). The CLaMS model data used in this study may be requested from the corresponding author. The monthly zonal-mean time series of SF_6-only AoA and multi-tracer AoA for dataset versions 3.6 and 5.2, as well as the CLaMS clock tracer AoA, are available at https://doi.org/10.5281/zenodo.21342696.

Author contributions. FV performed the investigation, data analysis, data curation, and visual representation. FP, JL, and PP initiated the study, conceptualized the core research questions, and contributed to writing the manuscript. JUG implemented the new trace gas species SF_6 and HCFC-22 in the CLaMS model. JL helped to develop the lower and upper boundary conditions of the six trace gases. JL and AM provided the aircraft and balloon measurements of SF_6. KAW, PES, and LNS contributed expertise on ACE-FTS. ST contributed expertise on long-term trends of age of air (AoA). MIH provided funding as co-PI of LOLIPOP. All authors participated in valuable discussions throughout the study, provided comments on the manuscript, and contributed to finalizing the paper.

Competing interests. At least one of the (co-)authors is a member of the editorial board of Atmospheric Chemistry and Physics.

Acknowledgements. We acknowledge the Atmospheric Chemistry Experiment Fourier Transform Spectrometer (ACE-FTS) team for the acquisition, processing, and provision of the trace-gas measurements used in this study. The Atmospheric Chemistry Experiment (ACE) is a Canadian-led mission mainly supported by the Canadian Space Agency (CSA). Our sincere thanks go to the Global Monitoring Laboratory of the National Oceanic and Atmospheric Administration (NOAA) for providing the essential mixing ratio time series that served as lower boundary conditions in the CLaMS simulations. We also gratefully acknowledge the MIPAS team for supplying the SF_6 and age-of-air (AoA) data sets, which were crucial for initializing the CLaMS simulations and defining the upper boundary condition for SF_6. We would like to express our appreciation to Nicole Thomas and Patrick Jöckel for their support and assistance in setting up the model simulations. Finally, we are deeply grateful for the computing time granted on the supercomputer JUWELS at the Jülich Supercomputing Centre (JSC), provided under the VSR project ID CLAMS-ESM, which was vital for the completion of the CLaMS simulations. AI tools were used solely for language editing and text polishing; the scientific content, analyses, and conclusions were produced by the authors.

Financial support. This study was funded by the Deutsche Forschungsgemeinschaft (DFG, German Research Foundation) — QUANTITEE – (grant no. 462476233) and extended through the European Space Agency (ESA) via the LOng-LIved greenhouse gas PrOducts Performances (LOLIPOP) project (under ESA contract no. 4000142090/23/I-NB)

https://doi.org/10.5194/egusphere-2026-4647
Preprint. Discussion started: 2 September 2026

References

Adcock, K. E., Fraser, P. J., Hall, B. D., Langenfelds, R. L., Lee, G., Montzka, S. A., Oram, D. E., Röckmann, T., Stroh, F., Sturges, W. T., Vogel, B., and Laube, J. C.: Aircraft-Based Observations of Ozone-Depleting Substances in the Upper Troposphere and Lower Stratosphere in and Above the Asian Summer Monsoon, Journal of Geophysical Research: Atmospheres, 126, e2020JD033 137, https://doi.org/https://doi.org/10.1029/2020JD033137, e2020JD033137 2020JD033137, 2021.

Andrews, A. E., Boering, K. A., Daube, B. C., Wofsy, S. C., Loewenstein, M., Jost, H., Podolske, J. R., Webster, C. R., Herman, R. L., Scott, D. C., Flesch, G. J., Moyer, E. J., Elkins, J. W., Dutton, G. S., Hurst, D. F., Moore, F. L., Ray, E. A., Romashkin, P. A., and Strahan, S. E.: Mean ages of stratospheric air derived from in situ observations of CO2, CH4, and N2O, Journal of Geophysical Research: Atmospheres, 106, 32 295–32 314, https://doi.org/https://doi.org/10.1029/2001JD000465, 2001.

Bernath, P. F., McElroy, C. T., Abrams, M. C., Boone, C. D., Butler, M., Camy-Peyret, C., Carleer, M., Clerbaux, C., Coheur, P.-F., Colin, R., DeCola, P., DeMazière, M., Drummond, J. R., Dufour, D., Evans, W. F. J., Fast, H., Fussen, D., Gilbert, K., Jennings, D. E., Llewellyn, E. J., Lowe, R. P., Mahieu, E., McConnell, J. C., McHugh, M., McLeod, S. D., Michaud, R., Midwinter, C., Nassar, R., Nichitiu, F., Nowlan, C., Rinsland, C. P., Rochon, Y. J., Rowlands, N., Semeniuk, K., Simon, P., Skelton, R., Sloan, J. J., Soucy, M.-A., Strong, K., Tremblay, P., Turnbull, D., Walker, K. A., Walkty, I., Wardle, D. A., Wehrle, V., Zander, R., and Zou, J.: Atmospheric Chemistry Experiment (ACE): Mission overview, Geophysical Research Letters, 32, https://doi.org/https://doi.org/10.1029/2005GL022386, 2005.

Bernath, P. F., Boone, C. D., Lecours, M. J., Crouse, J., Steffen, J., and Schmidt, M.: Global Satellite-Based Atmospheric Profiles from Atmospheric Chemistry Experiment SciSat Level 2 Processed Data, v5.2, 2004-2024, https://doi.org/10.20383/103.01245, 2025.

Boone, C., Bernath, P., Cok, D., Jones, S., and Steffen, J.: Version 4 retrievals for the atmospheric chemistry experiment Fourier transform spectrometer (ACE-FTS) and imagers, Journal of Quantitative Spectroscopy and Radiative Transfer, 247, 106 939, https://doi.org/https://doi.org/10.1016/j.jqsrt.2020.106939, 2020.

Boone, C., Bernath, P., and Lecours, M.: Version 5 retrievals for ACE-FTS and ACE-imagers, Journal of Quantitative Spectroscopy and Radiative Transfer, 310, 108 749, https://doi.org/https://doi.org/10.1016/j.jqsrt.2023.108749, 2023.

Boone, C. D., Nassar, R., Walker, K. A., Rochon, Y., McLeod, S. D., Rinsland, C. P., and Bernath, P. F.: Retrievals for the atmospheric chemistry experiment Fourier-transform spectrometer, Appl. Opt., 44, 7218–7231, https://doi.org/10.1364/AO.44.007218, 2005.

Boone, C. D., Walker, K. A., and Bernath, P. F.: Version 3 retrievals for the Atmospheric Chemistry Experiment Fourier Transform Spectrometer (ACE-FTS), in: ACE at 10: A Solar Occultation Anthology, Deepak Publishing, Hampton, Virginia, USA, ISBN 978-0-937194-54-9, 2013.

Castillo, A. E., Linz, M., Ray, E., Saunders, L. N., Walker, K. A., Stiller, G. P., Mooring, T. A., and Bourguet, S.: Developing tracer interrelationships to derive stratospheric age of air from satellite observations of nitrous oxide, EGUsphere, 2026, 1–30, https://doi.org/10.5194/egusphere-2026-1236, 2026.

Dubé, K., Tegtmeier, S., Ploeger, F., and Walker, K. A.: Hemispheric asymmetry in recent stratospheric age of air changes, Atmospheric Chemistry and Physics, 25, 1433–1447, https://doi.org/10.5194/acp-25-1433-2025, 2025.

Dutton, G. S., Hall, B. D., Dlugokencky, E. J., Lan, X., Madronich, M., Nance, J. D., and Petersen, K. M.: Combined Atmospheric Sulfur Hexafluoride Dry Air Mole Fractions from the NOAA GML Halocarbons Sampling Network, 1995–2026, https://doi.org/10.15138/TQ02-ZX42, [data set], 2026a.

https://doi.org/10.5194/egusphere-2026-4647
Preprint. Discussion started: 2 September 2026

Dutton, G. S., Hall, B. D., Montzka, S. A., Nance, J. D., Clingan, S. D., and Petersen, K. M.: Combined Atmospheric Chlorofluorocarbon-11 Dry Air Mole Fractions from the NOAA GML Halocarbons Sampling Network, 1977–2026, https://doi.org/10.15138/BVQ6-2S69, [data set], 2026b.

Dutton, G. S., Hall, B. D., Montzka, S. A., Nance, J. D., Clingan, S. D., and Petersen, K. M.: Combined Atmospheric Chlorofluorocarbon-12 Dry Air Mole Fractions from the NOAA GML Halocarbons Sampling Network, 1977–2026, https://doi.org/10.15138/PJ63-H440, [data set], 2026c.

Fischer, H., Birk, M., Blom, C., Carli, B., Carlotti, M., von Clarmann, T., Delbouille, L., Dudhia, A., Ehhalt, D., Endemann, M., Flaud, J. M., Gessner, R., Kleinert, A., Koopman, R., Langen, J., López-Puertas, M., Mosner, P., Nett, H., Oelhaf, H., Perron, G., Remedios, J., Ridolfi, M., Stiller, G., and Zander, R.: MIPAS: an instrument for atmospheric and climate research, Atmospheric Chemistry and Physics, 8, 2151–2188, https://doi.org/10.5194/acp-8-2151-2008, 2008.

Garny, H., Eichinger, R., Laube, J. C., Ray, E. A., Stiller, G. P., Bönisch, H., Saunders, L., and Linz, M.: Correction of stratospheric age of air (AoA) derived from sulfur hexafluoride (SF_6) for the effect of chemical sinks, Atmospheric Chemistry and Physics, 24, 4193–4215, https://doi.org/10.5194/acp-24-4193-2024, 2024a.

Garny, H., Ploeger, F., Abalos, M., Bönisch, H., Castillo, A. E., von Clarmann, T., Diallo, M., Engel, A., Laube, J. C., Linz, M., Neu, J. L., Podglajen, A., Ray, E., Rivoire, L., Saunders, L. N., Stiller, G., Voet, F., Wagenhäuser, T., and Walker, K. A.: Age of Stratospheric Air: Progress on Processes, Observations, and Long-Term Trends, Reviews of Geophysics, 62, e2023RG000 832, https://doi.org/https://doi.org/10.1029/2023RG000832, e2023RG000832 2023RG000832, 2024b.

Garny, H., Saunders, L., Voet, F., Ray, E., von Clarmann, T., Bönisch, H., Engel, A., Laube, J., Linz, M., Stiller, G., Wagenhäuser, T., and Walker, K. A.: Age of stratospheric air: observational data sets, https://doi.org/10.5281/zenodo.11267157, 2024c.

Grooß, J.-U. and Russell, J. M.: Technical Note: A stratospheric climatology for O_3, H_2O, CH_4, NO_x, HCl and HF derived from HALOE measurements, acp, 5, 2797–2807, 2005.

Grooß, J.-U.: Modelling of stratospheric chemistry based on HALOE/UARS satellite data, Ph.D. thesis, University of Mainz, 1996.

Haenel, F. J., Stiller, G. P., von Clarmann, T., Funke, B., Eckert, E., Glatthor, N., Grabowski, U., Kellmann, S., Kiefer, M., Linden, A., and Reddmann, T.: Reassessment of MIPAS age of air trends and variability, Atmospheric Chemistry and Physics, 15, 13 161–13 176, https://doi.org/10.5194/acp-15-13161-2015, 2015.

Hall, T. M. and Plumb, R. A.: Age as a diagnostic of stratospheric transport, Journal of Geophysical Research: Atmospheres, 99, 1059–1070, https://doi.org/https://doi.org/10.1029/93JD03192, 1994.

Hauck, M., Bönisch, H., Hoor, P., Keber, T., Ploeger, F., Schuck, T. J., and Engel, A.: A convolution of observational and model data to estimate age of air spectra in the northern hemispheric lower stratosphere, Atmospheric Chemistry and Physics, 20, 8763–8785, https://doi.org/10.5194/acp-20-8763-2020, 2020.

Hegglin, M. I. and Tegtmeier, S.: The SPARC Data Initiative: Assessment of stratospheric trace gas and aerosol climatologies from satellite limb sounders, ETH-Zürich, 2017.

Hegglin, M. I., Tegtmeier, S., Anderson, J., Bourassa, A. E., Brohede, S., Degenstein, D., Froidevaux, L., Funke, B., Gille, J., Kasai, Y., Kyrölä, E. T., Lumpe, J., Murtagh, D., Neu, J. L., Pérot, K., Remsberg, E. E., Rozanov, A., Toohey, M., Urban, J., von Clarmann, T., Walker, K. A., Wang, H.-J., Arosio, C., Damadeo, R., Fuller, R. A., Lingenfelser, G., McLinden, C., Pendlebury, D., Roth, C., Ryan, N. J., Sioris, C., Smith, L., and Weigel, K.: Overview and update of the SPARC Data Initiative: comparison of stratospheric composition measurements from satellite limb sounders, Earth System Science Data, 13, 1855–1903, https://doi.org/10.5194/essd-13-1855-2021, 2021.

Hersbach, H., Bell, B., Berrisford, P., Biavati, G., Horányi, A., Muñoz Sabater, J., Nicolas, J., Peubey, C., Radu, R., Rozum, I., Schepers, D., Simmons, A., Soci, C., Dee, D., and Thépaut, J.-N.: ERA5 hourly data on single levels from 1940 to present, https://doi.org/10.24381/cds.adbb2d47, [data set], 2023.

Hoppe, C. M., Hoffmann, L., Konopka, P., Grooß, J.-U., Ploeger, F., Günther, G., Jöckel, P., and Müller, R.: The implementation of the CLaMS Lagrangian transport core into the chemistry climate model EMAC 2.40.1: application on age of air and transport of long-lived trace species, Geoscientific Model Development, 7, 2639–2651, https://doi.org/10.5194/gmd-7-2639-2014, 2014.

Jaeglé, L., Wang, J., Oman, L., DeLand, M., and STRIVE Science Team: The STRIVE Earth System Explorer Mission Concept, in: EGU General Assembly 2025, https://doi.org/10.5194/egusphere-egu25-7598, presentation EGU25-7598, 2025.

Kida, H.: General Circulation of Air Parcels and Transport Characteristics Derived from a hemispheric GCM, Journal of the Meteorological Society of Japan. Ser. II, 61, 171–187, https://doi.org/10.2151/jmsj1965.61.2_171, 1983a.

Kida, H.: General Circulation of Air Parcels and Transport Characteristics Derived from a Hemispheric GCM, Journal of the Meteorological Society of Japan. Ser. II, 61, 510–523, https://doi.org/10.2151/jmsj1965.61.4_510, 1983b.

Kiefer, M.: Satellite-borne Remote Sensing of Trace Gases (SAT), MIPAS/ENVISAT Data, V5R SF6 121/224/225, https://www.imk-asf.kit.edu/english/308.php, last access: 28 February 2025, 2021.

Konopka, P., Tao, M., Ploeger, F., Diallo, M., and Riese, M.: Tropospheric mixing and parametrization of unresolved convective updrafts as implemented in the Chemical Lagrangian Model of the Stratosphere (CLaMS v2.0), Geoscientific Model Development, 12, 2441–2462, https://doi.org/10.5194/gmd-12-2441-2019, 2019.

Konopka, P., Tao, M., von Hobe, M., Hoffmann, L., Kloss, C., Ravegnani, F., Volk, C. M., Lauther, V., Zahn, A., Hoor, P., and Ploeger, F.: Tropospheric transport and unresolved convection: numerical experiments with CLaMS 2.0/MESSy, Geoscientific Model Development, 15, 7471–7487, https://doi.org/10.5194/gmd-15-7471-2022, 2022.

Lan, X., Tans, P., Thoning, K., and NOAA Global Monitoring Laboratory: NOAA Greenhouse Gas Marine Boundary Layer Reference – CH_4, https://doi.org/10.15138/DVNP-F961, [data set], 2024a.

Lan, X., Tans, P., Thoning, K., and NOAA Global Monitoring Laboratory: NOAA Greenhouse Gas Marine Boundary Layer Reference – N_2O, https://doi.org/10.15138/DVNP-F961, [data set], 2024b.

Lan, X., Tans, P., Thoning, K., and NOAA Global Monitoring Laboratory: NOAA Greenhouse Gas Marine Boundary Layer Reference - SF6, https://doi.org/10.15138/DVNP-F961, 2024c.

Laube, J. C., Leedham Elvidge, E. C., Adcock, K. E., Baier, B., Brenninkmeijer, C. A. M., Chen, H., Droste, E. S., Grooß, J.-U., Heikkinen, P., Hind, A. J., Kivi, R., Lojko, A., Montzka, S. A., Oram, D. E., Randall, S., Röckmann, T., Sturges, W. T., Sweeney, C., Thomas, M., Tuffnell, E., and Ploeger, F.: Investigating stratospheric changes between 2009 and 2018 with halogenated trace gas data from aircraft, AirCores, and a global model focusing on CFC-11, Atmospheric Chemistry and Physics, 20, 9771–9782, https://doi.org/10.5194/acp-20-9771-2020, 2020.

Leedham Elvidge, E. C., Bönisch, H., Brenninkmeijer, C. A. M., Engel, A., Fraser, P. J., Gallacher, E., Langenfelds, R., Mühle, J., Oram, D. E., Ray, E. A., Ridley, A. R., Röckmann, T., Sturges, W. T., Weiss, R. F., and Laube, J. C.: Evaluation of stratospheric age of air from CF_4, C_2F_6, C_3F_8, CHF_3, HFC-125, HFC-227ea and SF_6; implications for the calculations of halocarbon lifetimes, fractional release factors and ozone depletion potentials, Atmospheric Chemistry and Physics, 18, 3369–3385, https://doi.org/10.5194/acp-18-3369-2018, 2018.

Linz, M., Plumb, R. A., Gerber, E. P., Haenel, F. J., Stiller, G., Kinnison, D. E., Ming, A., and Neu, J. L.: The strength of the meridional overturning circulation of the stratosphere, Nature Geoscience, 10, 663–667, 2017.

https://doi.org/10.5194/egusphere-2026-4647
Preprint. Discussion started: 2 September 2026

Mahieu, E., Chipperfield, M., Notholt, J., Reddmann, T., Anderson, J., Bernath, P., Blumenstock, T., Coffey, M., Dhomse, S., Feng, W., et al.: Recent Northern Hemisphere stratospheric HCl increase due to atmospheric circulation changes, Nature, 515, 104–107, 2014.

McKenna, D. S., Grooß, J.-U., Günther, G., Konopka, P., Müller, R., Carver, G., and Sasano, Y.: A new Chemical Lagrangian Model of the Stratosphere (CLaMS) 2. Formulation of chemistry scheme and initialization, J. Geophys. Res., 107, https://doi.org/10.1029/2000JD000113, 2002a.

McKenna, D. S., Konopka, P., Grooß, J.-U., Günther, G., Müller, R., Spang, R., Offermann, D., and Orsolini, Y.: A new Chemical Lagrangian Model of the Stratosphere (CLaMS) 1. Formulation of advection and mixing, J. Geophys. Res., 107, https://doi.org/10.1029/2000JD000114, 2002b.

Montzka, S., McFarland, M., Andersen, S., Miller, B., Fahey, D., Hall, B., Hu, L., Siso, C., and Elkins, J.: Recent trends in global emissions of hydrochlorofluorocarbons and hydrofluorocarbons: Reflecting on the 2007 adjustments to the Montreal Protocol, The Journal of Physical Chemistry A, 119, 4439–4449, https://doi.org/10.1021/jp512570h, 2015.

NOAA Global Monitoring Laboratory: HCFC-22 Measurements from Flask Samples Analyzed by GCMS, https://gml.noaa.gov/data/dataset.php?item=hcfc22-hats-flask, [data set], 2026.

Pedregosa, F., Varoquaux, G., Gramfort, A., Michel, V., Thirion, B., Grisel, O., Blondel, M., Prettenhofer, P., Weiss, R., Dubourg, V., Vanderplas, J., Passos, A., Cournapeau, D., Brucher, M., Perrot, M., and Édouard Duchesnay: Scikit-learn: Machine Learning in Python, Journal of Machine Learning Research, 12, 2825–2830, http://jmlr.org/papers/v12/pedregosa11a.html, 2011.

Ploeger, F. and Garny, H.: Hemispheric asymmetries in recent changes in the stratospheric circulation, Atmospheric Chemistry and Physics, 22, 5559–5576, https://doi.org/10.5194/acp-22-5559-2022, 2022.

Ploeger, F., Günther, G., Konopka, P., Fueglistaler, S., Müller, R., Hoppe, C., Kunz, A., Spang, R., Grooß, J.-U., and Riese, M.: Horizontal water vapor transport in the lower stratosphere from subtropics to high latitudes during boreal summer, Journal of Geophysical Research: Atmospheres, 118, 8111–8127, https://doi.org/https://doi.org/10.1002/jgrd.50636, 2013.

Ploeger, F., Diallo, M., Charlesworth, E., Konopka, P., Legras, B., Laube, J. C., Grooß, J.-U., Günther, G., Engel, A., and Riese, M.: The stratospheric Brewer–Dobson circulation inferred from age of air in the ERA5 reanalysis, Atmospheric Chemistry and Physics, 21, 8393–8412, https://doi.org/10.5194/acp-21-8393-2021, 2021.

Pommrich, R., Müller, R., Grooß, J.-U., Konopka, P., Ploeger, F., Vogel, B., Tao, M., Hoppe, C. M., Günther, G., Spelten, N., Hoffmann, L., Pumphrey, H.-C., Viciani, S., D'Amato, F., Volk, C. M., Hoor, P., Schlager, H., and Riese, M.: Tropical troposphere to stratosphere transport of carbon monoxide and long-lived trace species in the Chemical Lagrangian Model of the Stratosphere (CLaMS), gmd, pp. 2895–2916, 2014.

Ray, E. A., Moore, F. L., Rosenlof, K. H., Davis, S. M., Sweeney, C., Tans, P., Wang, T., Elkins, J. W., Bönisch, H., Engel, A., Sugawara, S., Nakazawa, T., and Aoki, S.: Improving stratospheric transport trend analysis based on SF6 and CO2 measurements, Journal of Geophysical Research: Atmospheres, 119, 14,110–14,128, https://doi.org/https://doi.org/10.1002/2014JD021802, 2014.

Ray, E. A., Portmann, R. W., Yu, P., Daniel, J., Montzka, S. A., Dutton, G. S., Hall, B. D., Moore, F. L., and Rosenlof, K. H.: The influence of the stratospheric Quasi-Biennial Oscillation on trace gas levels at the Earth's surface, Nature Geoscience, 13, 22–27, 2020.

Ray, E. A., Moore, F. L., Garny, H., Hintsa, E. J., Hall, B. D., Dutton, G. S., Nance, D., Elkins, J. W., Wofsy, S. C., Pittman, J., Daube, B., Baier, B. C., Li, J., and Sweeney, C.: Age of air from in situ trace gas measurements: insights from a new technique, Atmospheric Chemistry and Physics, 24, 12 425–12 445, https://doi.org/10.5194/acp-24-12425-2024, 2024.

Ray, E. A., Baier, B. C., Moore, F. L., Garny, H., Jesswein, M., Li, J., Hintsa, E. J., Hall, B. D., Dutton, G. S., Nance, D., et al.: Observed stratospheric mean age decrease consistent with circulation acceleration, Nature Geoscience, pp. 1–6, 2026.

https://doi.org/10.5194/egusphere-2026-4647
Preprint. Discussion started: 2 September 2026

Saunders, L. N., Walker, K. A., Stiller, G. P., von Clarmann, T., Haenel, F., Garny, H., Bönisch, H., Boone, C. D., Castillo, A. E., Engel, A., Laube, J. C., Linz, M., Ploeger, F., Plummer, D. A., Ray, E. A., and Sheese, P. E.: Age of air from ACE-FTS measurements of sulfur hexafluoride, Atmospheric Chemistry and Physics, 25, 4185–4209, https://doi.org/10.5194/acp-25-4185-2025, 2025.

Sheese, P. E., Boone, C. D., and Walker, K. A.: Detecting physically unrealistic outliers in ACE-FTS atmospheric measurements, Atmospheric Measurement Techniques, 8, 741–750, https://doi.org/10.5194/amt-8-741-2015, 2015.

Stiller, G. P., von Clarmann, T., Höpfner, M., Glatthor, N., Grabowski, U., Kellmann, S., Kleinert, A., Linden, A., Milz, M., Reddmann, T., Steck, T., Fischer, H., Funke, B., López-Puertas, M., and Engel, A.: Global distribution of mean age of stratospheric air from MIPAS SF_6 measurements, Atmospheric Chemistry and Physics, 8, 677–695, https://doi.org/10.5194/acp-8-677-2008, 2008.

Stiller, G. P., von Clarmann, T., Haenel, F., Funke, B., Glatthor, N., Grabowski, U., Kellmann, S., Kiefer, M., Linden, A., Lossow, S., and López-Puertas, M.: Observed temporal evolution of global mean age of stratospheric air for the 2002 to 2010 period, Atmospheric Chemistry and Physics, 12, 3311–3331, https://doi.org/10.5194/acp-12-3311-2012, 2012.

Stiller, G. P., Fierli, F., Ploeger, F., Cagnazzo, C., Funke, B., Haenel, F. J., Reddmann, T., Riese, M., and von Clarmann, T.: Shift of subtropical transport barriers explains observed hemispheric asymmetry of decadal trends of age of air, Atmospheric chemistry and physics, 17, 11 177–11 192, https://doi.org/10.5194/acp-17-11177-2017, 12.04.05; LK 01, 2017.

Strahan, S. E., Smale, D., Douglass, A. R., Blumenstock, T., Hannigan, J. W., Hase, F., Jones, N. B., Mahieu, E., Notholt, J., Oman, L. D., Ortega, I., Palm, M., Prignon, M., Robinson, J., Schneider, M., Sussmann, R., and Velazco, V. A.: Observed Hemispheric Asymmetry in Stratospheric Transport Trends From 1994 to 2018, Geophysical Research Letters, 47, e2020GL088 567, https://doi.org/https://doi.org/10.1029/2020GL088567, e2020GL088567 2020GL088567, 2020.

Tegtmeier, S., Hegglin, M. I., Anderson, J., Funke, B., Gille, J., Jones, A., Smith, L., von Clarmann, T., and Walker, K. A.: The SPARC Data Initiative: comparisons of CFC-11, CFC-12, HF and SF_6 climatologies from international satellite limb sounders, Earth System Science Data, 8, 61–78, https://doi.org/10.5194/essd-8-61-2016, 2016.

Vervalcke, S., Errera, Q., Eichinger, R., Reddmann, T., Chabrillat, S., Op de beeck, M., Stiller, G., and Mahieu, E.: Atmospheric lifetime of sulphur hexafluoride (SF_6) and five other trace gases in the BASCOE model driven by three reanalyses, Atmospheric Chemistry and Physics, 26, 391–409, https://doi.org/10.5194/acp-26-391-2026, 2026.

Voet, F., Ploeger, F., Laube, J., Preusse, P., Konopka, P., Grooß, J.-U., Ungermann, J., Sinnhuber, B.-M., Höpfner, M., Funke, B., Wetzel, G., Johansson, S., Stiller, G., Ray, E., and Hegglin, M. I.: On the estimation of stratospheric age of air from correlations of multiple trace gases, Atmospheric Chemistry and Physics, 25, 3541–3565, https://doi.org/10.5194/acp-25-3541-2025, 2025.

Volk, C. M., Elkins, J. W., Fahey, D. W., Dutton, G. S., Gilligan, J. M., Loewenstein, M., Podolske, J. R., Chan, K. R., and Gunson, M. R.: Evaluation of source gas lifetimes from stratospheric observations, Journal of Geophysical Research: Atmospheres, 102, 25 543–25 564, https://doi.org/https://doi.org/10.1029/97JD02215, 1997.

Zhang, J., Yang, Y., and Ding, J.: Information criteria for model selection, WIREs Computational Statistics, 15, e1607, https://doi.org/https://doi.org/10.1002/wics.1607, 2023.